Exploration of Surface Plasmon-Assisted Catalysis (SPAC) as a New Route for Heterogeneous Catalysis

By

Melanie Dawn Davidson

A Thesis Submitted to
Saint Mary's University, Halifax, Nova Scotia
In Partial Fulfilment of the Requirements for the Degree of
Bachelor of Science with Honours in Chemistry

April 2017, Halifax, Nova Scotia

Copyright Melanie Dawn Davidson, 2017

Certification

Exploration of Surface Plasmon-Assisted Catalysis (SPAC) as a New Route for Heterogeneous Catalysis

I hereby certify that this thesis was completed by Melanie Dawn Davidson in partial fulfillment for the requirements of the Degree of Bachelor of Science with Honours in Chemistry at Saint Mary's University and I certify that this is truly the original work carried out by Melanie Dawn Davidson.

Thesis Supervisor

Dr. Christa L. Brosseau

_____

Chairperson of the Chemistry Department

Dr. Robert Singer

_____

Date: April 21, 2017

Abstract

Exploration of Surface Plasmon-Assisted Catalysis (SPAC) as a New Route for

Heterogeneous Catalysis

by

Melanie Dawn Davidson

Plasmonics is the study of the interactions between the free electrons of a metal, and the electric field component of light. In the presence of the oscillating electronic field, the free electrons in the metal oscillate collectively, resulting in a localized surface plasmon resonance (LSPR). This LSPR is the reason for the enhanced spectra of surface enhanced Raman spectroscopy (SERS) compared to Raman spectroscopy. A commonly used Raman reporter is 4-aminothiophenol (4-ATP), which has been well studied. 4-ATP is known to undergo a surface catalytic coupling reaction to produce an aromatic azo species: 4,4'-dimercaptoazobenzene (4,4'-DMAB). This work explores the generality of the surface plasmon-assisted catalysis (SPAC) by studying the constitutional isomers, the 2- and 3- constituents of 4-ATP. The reusability of the catalyst (electrode set-up) is also tested to suggest a new route for heterogeneous catalysis, and further tested if the oxidative product, 4,4'-DMAB, could be obtained once removed.

April 21, 2016

Acknowledgements

I would like thank Dr. Christa Brosseau for being my research supervisor and for all her help along the way. Not only did she offer me support and encouragement, but also advice and guidance that I will always keep with me. Special thanks also to all past and present members of the Brosseau research group, especially Osai Clarke, Reem Karaballi and Taylor Lynk who not only helped with my work but helped keep me sane.

I would also like to thank Darlene Goucher, Alyssa Doué, and the entire chemistry department for their continuous support. I would like to especially thank Dr. Kai Ylijoki, Dr. Robert Singer, and Kyle Awalt for their help with the organic synthesis part of my work and always entertaining my sometimes ridiculous questions. Also, thanks to Yaoting Zhang for his DFT and theoretical work.

Finally, I would like to acknowledge my family and friends who have supported me through this entire process and made my time at SMU a little brighter.

Table of Contents   Page #

List of Abbreviations

2-ATP	2-Aminothiophenol
2,2'-DMAB	2,2'-Dimecaptoazobenzene
3-ATP	3-Aminothiophenol
3,3'-DMAB	3,3'-Dimercaptoazobenzene
4-ATP	4-Aminothiophenol
4,4'-DMAB	4,4'-Dimercaptoazobenzene
4-NBT	4-nitrobenzenethiol
CE	Counter Electrode
CV	Cyclic Voltammetry
DBSCA	Double Step Chronoamperometry
EC-SERS	Electrochemical Surface Enhanced Raman Spectroscopy
LSP	Localised Surface Plasmon
LSPR	Localised Surface Plasmon Resonance
NP	Nanoparticle
OCP	Open Circuit Potential
PSP	Propagating Surface Plasmon
PSPR	Propagating Surface Plasmon Resonance
RE	Reference Electrode
SEM	Scanning Electron Microscopy
SERS	Surface Enhanced Raman Spectroscopy
SP	Surface Plasmon
SPAC	Surface Plasmon Assisted Catalysis
SPEs	Screen Printed Carbon Electrodes
SPR	Surface Plasmon Resonance
THF	Tetrahydrofuran
WE	Working Electrode

List of Figures

List of Tables

Chapter 1: Introduction

The molecule 4-Aminothiophenol (4-ATP) is commonly used in Raman and SERS practices as a probe molecule. In addition to being a strong Raman reporter, 4-ATP undergoes a surface plasmon assisted catalysis (SPAC) reaction during SERS experiments to form the catalytic oxidation product 4,4'-dimercaptoazobenzene (4,4'-DMAB). This catalysis pathway was discovered in 2010, along with 4-nitrobenzenethiol (4-NBT) which also undergoes a similar catalytic reaction to form the common product, 4,4'-DMAB.[3,6] Chapter 2 will give a literature review of the topics covered in this work and a brief history on the SPAC reaction. Chapters 3 and 4 will give an overview on techniques and theories needed to complete the experiments and understand the results being presented. This thesis delves into the current understanding of the SPAC reaction and looks to see if it is ubiquitous by examining isomers of 4-ATP, such as 2-aminothiophenol (2-ATP) and 3-aminothiophenol (3-ATP). 4-ATP is also being examined as its role as a Raman probe during SERS studies, wondering if the conversion to 4,4'-DMAB on the surface of the nanoparticles could interfere with its ability to be a quantitative marker. The SPAC reaction was also tested to see if could be a new route for heterogenous catalysis by the isolation and collection of 4,4'-DMAB. Electrochemical studies on 4-ATP were conducted to create and then anodically desorb 4,4'-DMAB from the surface of an electrode. Chapter 5 will show all results and findings and will discuss the relevance. Finally, chapter 6 will conclude the results and importance of this work while showing work to continue this project in the future.

Chapter 2: Literature Review

2.1 Catalysis

2.1.1 Catalysis Overview

Catalysis deals with reaction kinetics, a catalyst provides an alternate pathway with a lower activation energy which allows the reaction to proceed at a quicker rate. Without catalysis these reactions would either not occur, or would occur with slower rates and lower efficiencies.[7] This can be demonstrated by the reaction coordinate shown in Figure 2.1, which shows the lower activation energy of a catalyzed reaction.
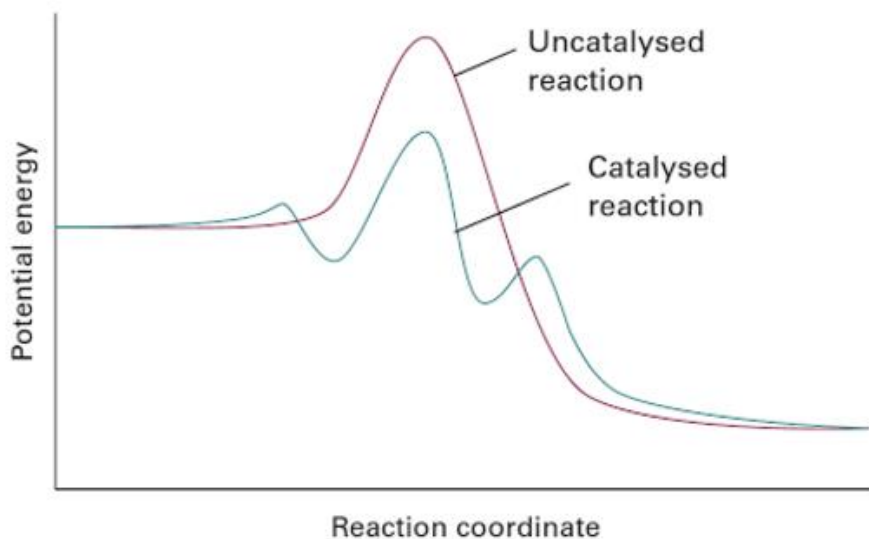
Figure 2.1: The reaction coordinate of an uncatalyzed reaction overlaid with a catalysed reaction.[8]

Another important factor in catalysis is that the catalyst, the species that facilitates the new chemical reaction, is not consumed in the reaction. Having the catalytic step and the entire reaction proceed repeatedly without having the catalyst consumed allows catalysis to be seen in a green and reusable fashion. This allows catalysis to also be viewed as cost efficient, which explains its wide use in the industrial industry.[7] There are two main types of catalysis: homogenous and heterogenous. Homogenous catalysis is when the catalyst is

in the same phase as the reactants and products.[9] Figure 2.2a shows an example of homogeneous catalysis through a hydrogenation reaction. This reaction has hydrogen gas in the reaction equation, however some of the gas dissolves in the liquid and give rise to its participation in the catalytic cycle.[10] Conversely, heterogenous catalysis is when the catalyst and substrate are in different phases.[10] The Haber-Bosch ammonia synthesis is a classic example of heterogeneous catalysis, as shown in Figure 2.2b. The gaseous nitrogen and hydrogen are passed over solid magnetite (Fe) beds allowing ammonia to be produced on an industrial scale.[9,10] This thesis work deals only with heterogeneous catalysis as it pertains to the research objectives.
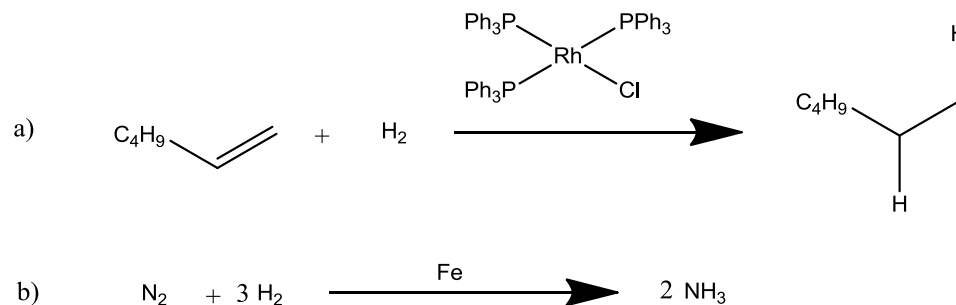
Figure 2.2 a Hydrogenation of 1-hexene to hexane in the presence of Wilkinson's catalyst, Rh[P(Ph)$_3$]$_3$Cl; **b** Haber-Bosch ammonia synthesis from gaseous nitrogen and hydrogen.

Two cases where catalysis can lessen or adversely affect the reaction are in catalyst inhibition or catalyst poising. Inhibition is commonly associated with biocatalytic processes but can affect both homogeneous and heterogeneous catalysis as well.[10] Competitive inhibition is when two molecules compete for the same active site on catalyst surface, therefore a competitive inhibitor is any chemical species that can bind to the same site as the substrate.[10] Noncompetitive inhibition does not compete with the substrate, but the noncompetitive inhibitor binds to an allosteric site and thus changes the

properties of the active site.[10] Changing the property of the active site can slow or even stop catalytic activity, hence inhibiting the reaction. Catalyst poisoning is essentially a bad case of inhibition, this is when an inhibitor irreversibly binds to the catalyst and slows catalysis until it eventually stops with enough poisoning.[10]

2.1.2 Nanoscale Heterogeneous Catalysis

As explained above, heterogeneous catalysis involves a substrate and catalyst in different phases. Most popularly, this reaction involves adsorption of reactants from a solution phase onto a solid surface, after which a surface reaction of the adsorbed species takes place, followed by desorption of the reaction products back into the solution phase.[11] As described in the above section, substrates bond onto the surface of the solid catalyst and reacts accordingly in order to create a new, catalytic reaction pathway. The more surface area available on the solid surface, the more reactants are able to be adsorbed, which enhances the catalytic ability.[12,13] As this material shrinks and starts measuring in the nanoscale range, we are seeing even greater enhancements, this is due to the exponential size of surface area and the amount of particles available. When below 10 nm these particles adapt properties more like that of a single atom thus further adding to its catalytic abilities.[12]

In recent years, the research topic of nanoscale catalysis has only grown in popularity. When a Web of Science publication report on the topic "nanoscale catalysis" (Figure 2.3) is generated, it is apparent that the subject is developing and advancing. With some of the most recent publications involving nano-modified organic frameworks,[14] nanocrystalline zinc coordination polymers,[15] and nanostructured silver and copper fabrics used in localized surface plasmon resonance.[16]
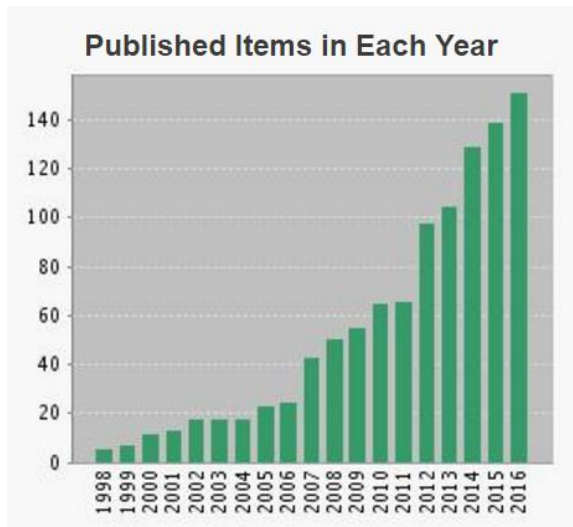
Figure 2.3: Web of Science number of publications found for the topic of "nanoscale catalysis" from 1998-2016. Created 04-06-17.

2.2 Plasmonics

Plasmonics is the field of research concerned with the light-matter interaction between the collective oscillation of free electrons of a metal and an incident electromagnetic field. This results in localised surface plasmons(LSP) and propagating surface plasmons (PSP).[17] If the frequency of the electromagnetic wave matches the frequency of electron oscillation from the metal nanostructures, a surface plasmon resonance (SPR) can result. This resonance causes a great enhancement of the electric field at, or near the surface of the metal.[1,17]

Surface plasmons can be classified as one of two types: localized surface plasmon (LSP), or propagating surface plasmon (PSP). LSPs are described in metals that are nanoscale in all dimensions, such as a nanosphere. Contrarily, PSPs are described in metals that are nanoscale in one or two dimensions, such as a nanofilm and a nanowire respectively.[1] Both LSPs and PSPs give rise to resonance, accurately named localized surface plasmon resonance (LSPR) and propagating surface plasmon resonance (PSPR),

respectively. This thesis deals only in LSPs and LSPR as it pertains to the research objective.

LSPR can be most simply described through Mie theory by the way of the following equation 2.1, where C_{ext} is the extinction cross-section, ε is the complex dielectric function for the metal which includes both a real (ε_r) and an imaginary component (ε_i), and λ is the excitation wavelength. The dielectric function of a material varies with changing excitation wavelengths of light, as it expresses the unique interaction between its electrons and the light .[1]

$$C_{ext} = \frac{24\pi^2 R^3 \varepsilon_m^{3/2}}{\lambda} \left[\frac{\varepsilon_i}{(\varepsilon_r + 2\varepsilon_m)^2 + \varepsilon_i^2} \right] \qquad 2.1$$

Since the interaction of light and a metal nanoparticle is highly dependent on its dielectric properties, ε_r and ε_i, when the denominator in the bracketed portion of the equation approaches zero, C_{ext} will become very large and its optical absorption and scattering becomes very strong.[1] To achieve this condition a material with a negative real component, and a small, positive imaginary component of the complex dielectric function are required.[1] This is only possible for metals, and only reigns true for some metals, such as Ag, and Au, as shown in Figure 2.4 which compares the dielectric constants of Ag and Au to those of Si.
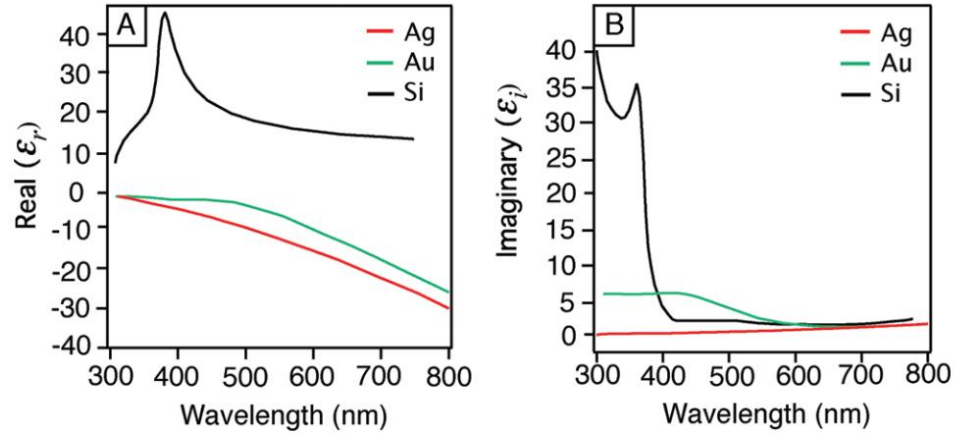
Figure 2.4: Plots of the real (A) and imaginary (B) components of the dielectric function of Ag, Au, and Si (Reproduced with permission).[1]

When comparing metals for plasmon strength in the visible region, it is necessary to recognize the quality factor, Q, as described in equation 2.2. The SP strength is directly proportional to Q, where large Q values mean strong SP and small Q values mean weak SP with a small C_{ext}.[10] For plasmonic applications to be relized, the Q value should be above ~10.[1]

$$Q = \frac{w(\frac{d\varepsilon_r}{dw})}{2(\varepsilon_i)^2} \qquad\qquad 2.2$$

Figure 2.5 shows the plot of Q values against wavelength of various metals in order to compare their plasmonic strengths and abilities. This spectrum shows that Ag has the greatest plasmonic strength over the visible spectral range, highlighting why silver is the most commonly used substrate in plasmonic applications. It is also apparent that Au, Cu, and Al are alternate possibilities for plasmonic substrates. However they are not as versatile as they cover only certain wavelengths, shown most strongly by Al which is only plasmoinc in the ultraviolet range, and both Au and Cu are only plasmonic above ~600nm due to interfering interband transitions.[1]
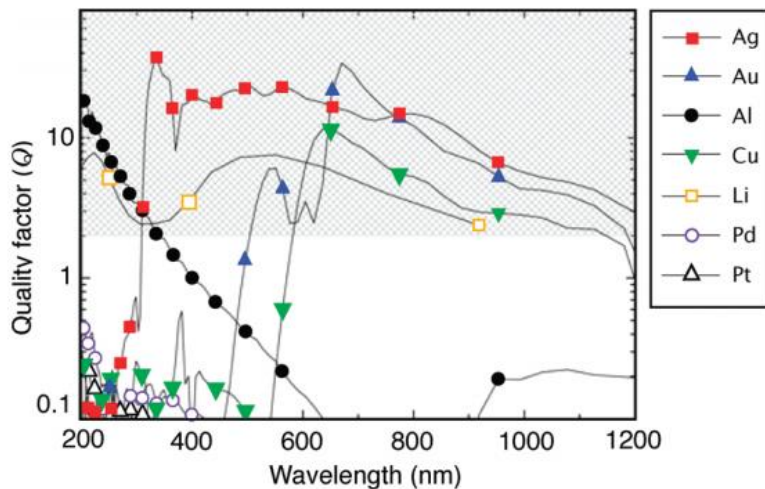
Figure 2.5: Quality factor (Q) of the LSPR for a metal/air interface of various metals. The shaded area represents the area of interest for many plasmonic applications (Reproduced with permission).[1]

This research uses both Ag and Au as plasmonic substrates as they are, historically, the most commonly used and are plasmonic over large wavelength ranges. Another enticing reason to use these metals include their physical properties, such as low reactivity (in comparison to Li), lack of extensive air-oxidation (such as Cu), and the ease with which controlled nanostructures can be synthesized.[1]

2.3 Surface Plasmonic Assisted Catalysis

2.3.1 SPAC Overview

Surface Plasmon Assisted Catalysis (SPAC) uses the decay of surface plasmons to aid in the catalysis of reactions near the metal surface. Surface plasmons lose their energy in one of two ways; by absorption into the metal, or by radiation into free space.[18] When a plasmon decays, it creates "hot" electron and hole pairs along the metal surface, which are thought to be the main component of the SPAC mechanism.[18,19] These "hot" electrons provide two or three important contributions to the SPAC mechanism; the first

is that additional electrons may be needed in the catalytic reaction, therefore the "hot" electrons are donated into the reaction as shown in Figure 2.6. The other contributions are due to the transfer of the "hot" electrons, with kinetic energy above the Fermi level, jumping to the unoccupied resonant energy level of chemical reactants near the metal surface.[18] This occupation of a resonance level changes the equilibrium potential of the surface from neutral to a temporary negative ion situation. The energy from the "hot" electrons can also be transferred to the intramolecular vibrational energy, which in both these cases can decrease the activation energy barrier for the chemical reaction, creating a catalytic pathway.[18]
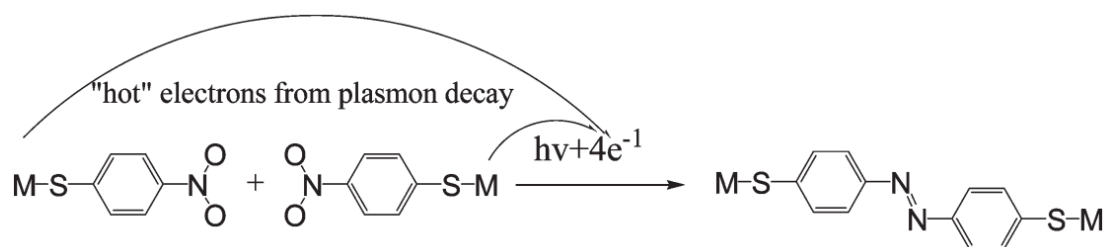
Figure 2.6: SPAC reaction pathway where "hot" electrons are donated into the reaction.[2]

2.3.2 4-Aminothiophenol

The first molecule known to go through a SPAC process was 4-aminothiophenol (4-ATP).[3] The molecule 4-ATP is a popular probe in Raman spectroscopy and, more importantly, surface-enhanced Raman spectroscopy (SERS), because it is a strong Raman reporter and has strong interactions with both Ag and Au through the formation of a metal–sulfur bond .[3] 4-ATP was first used as a probe molecule in 1994 by Osawa et al.[20] This group characterized the band assignments of 4-ATP and noted the different Raman spectra that this molecule produced when adsorbed to a nanoscale Ag surface compared

to its solid form.[20] This is the first time the notion of b_2 modes were expressed for the appearance of unexpected peaks in the SERS signal of 4-ATP.

In these studies of 4-ATP, three additional peaks (1140, 1391, and 1440 cm^{-1}) were noted in the SERS spectrum, which were not expected of this molecule based on the normal Raman spectrum.[3] These peaks were attributed and widely accepted as the b_2 modes of 4-ATP. However, when looked at computationally, the three peaks were from another molecule, that of the catalytic oxidation product 4,4'-dimercaptoazobenzene (4,4'-DMAB).[3,21,22] This was confirmed as the most probable cause of the additional peaks after 4,4'-DMAB was synthesized independently and then characterized.[3] The synthesis started with aniline which was reacted with I_2 in $NaHCO_3/H_2O$ for half an hour to afford 4-iodoaniline. Before further reaction, 4-iodoaniline was decolourized with $NaHSO_3$ and sublimed. This sublimation product was then reacted with $NaBO_3 \cdot 4H_2O/H_3BO_3$ in acetic acid at 50-60°C for six hours to afford 4,4'-diiodoazobenzene after recrystallization in THF. The 4,4'-diiodoazobenzene product then undergoes a Grignard reaction by first reacting with magnesium in THF at 60°C for 24 hours; sulfur was then added to the mixture and allowed to react for an additional 12-25 hours. After workup, the resulting mixture was quenched with saturated NH_4Cl/H_2O and acidified with aqueous HCl. This product is recrystallized and thus affords the intended product of 4,4'-dimercaptoazobenzene (4,4'-DMAB), as shown in Figure 2.7.[3]
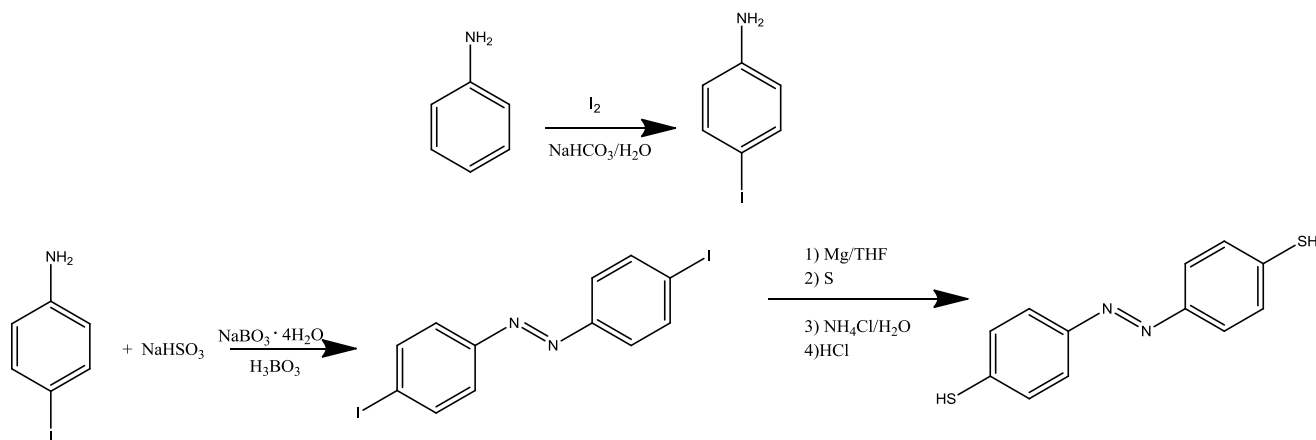
Figure 2.7: Reaction sheme for the synthesis of 4,4'-dimercaptoazobenzene from aniline as described by Huang et al. [3]

Once it was known that 4,4'-DMAB was produced from 4-ATP via this novel catalytic route, SPAC became a highly topical and investigated subject in the literature. It was noted that similar process occurred for the molecule 4-Nitrobenzenethiol (4-NBT), in which an azo product 4,4'-DMAB could be observed through the surface-enhanced Raman spectrum.[6]

As of yet, the SPAC conversion of 4-ATP to 4,4'-DMAB has been studied by many groups around the world. These studies include analysis on different metals (such as Ag, Au, and Cu)[2], in presence of different additives (NO_2^- and O_2)[23,24], and at different wavelengths (633 nm, 632.8 nm, 532 nm, 514.5 nm, 239.5 nm, 282.3 nm, 299.1 nm, 309.1 nm, and 3199.9 nm)[2,19,20]. All these studies have help further the understanding of the SPAC process, and even though the mechanism is still disputed, there are theories. The most accepted mechanistic process can be seen in Figure 2.8 and features a cationic radical species. This cationic radical species has been recently explored by Jiang et al., showing possible resonance structures and comparing between the isomers 2-ATP and 3-ATP.[5]

This chapter discussed the history and recent applications of both plasmonics and the SPAC reaction. As it is well known, 4-ATP undergoes the SPAC conversion to the oxidative product 4,4'-DMAB. This transformation is the basis for the following work, looking again at this molecule and extending out to isomers to examine if the SPAC process can expanded to include similar molecules. The reusability of the catalyst (electrode set-up) is also tested to suggest a new route for heterogeneous catalysis, and further tested if the oxidative product could be obtained once removed.

Chapter 3: Theory

3.1 Raman Spectroscopy

Raman spectroscopy is a common vibrational technique that is based on the inelastic scattering of monochromatic light. Light can interact with matter in one of three ways; the photons that make up the light may be absorbed, emitted or scattered by atoms and molecules.[25] When light is scattered by a molecule it can be scattered in different ways: Rayleigh, anti-Stokes and Stokes scattering, all shown in Figure 3.1. Rayleigh scattering, also known as elastic scattering occurs most frequently. This type of scattering has the excited molecule returning back to its ground state with no net energy transfer, and therefore does not contain any vibrational information.[26] Anti-Stokes and Stokes, collectively known as Raman scattering, undergo a net energy gain and loss respectively. In most cases molecules are present in the ground state, therefore the Stokes Raman scattering is more probable and thus more useful.[26] Every molecule will scatter light differently based on their molecular structure which therefore allows Raman spectroscopy to be specific and provide chemical 'fingerprints' used to identify molecules. However, since only one in every 10^6-10^8 photons are Raman scattered, it is an inherently weak process.[26,27] As a results, Raman spectroscopy has historically only been useful in the analysis of bulk powders and neat liquids, due to this lack of sensitivity. This process can be greatly enhanced, up to 10^4-10^{11} orders of magnitude, by using a technique named surface enhanced Raman spectroscopy (SERS).[27]
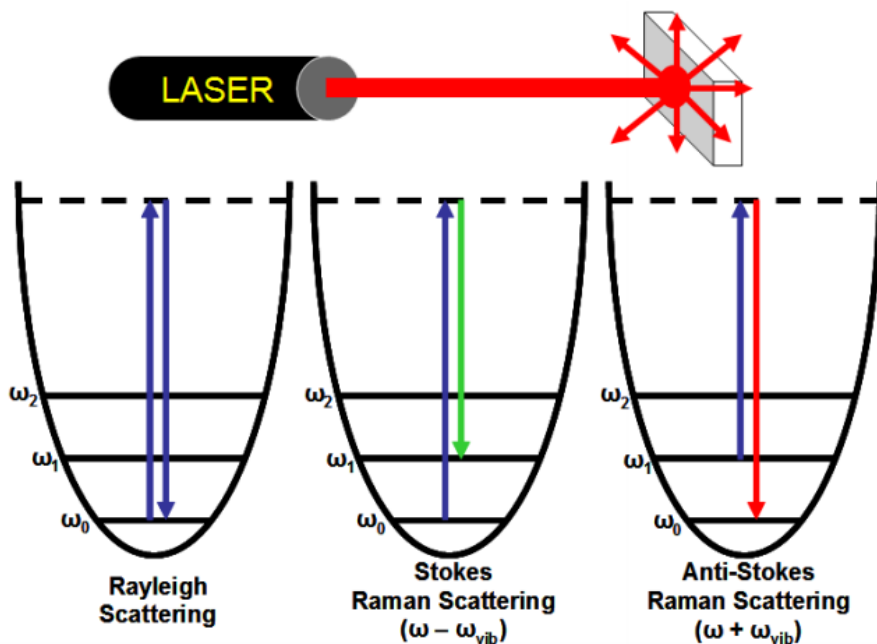
Figure 3.1: Diagram which shows the different light scattering modes: Rayleigh, Stokes, and anti-Stokes scattering.

3.2 Surface Enhanced Raman Spectroscopy (SERS)

SERS was first reported in 1974 by Fleishman et al. where it was shown that pyridine and other molecules display an enhancement in Raman signal when adsorbed onto an electrochemically roughened metal surface.[28] After this was noted, Van Duyne and Jeanmaire looked into the factors that would affect the intensity of the Raman signal and reported that source of the enhancement was not due solely to the increase of surface area, but that most of the signal increase was due to an enhanced electromagnetic field on the surface on the nanoscale metal.[29] This technique is referred to as surface-enhanced Raman spectroscopy (SERS), which exploits this enhancement of Raman signal of molecules present on roughened nanoscale metal surfaces, most commonly Ag, Au, and Cu.[30,27] The magnitude of the Raman signal can be enhanced 10^4-10^{11} orders of magnitude by using this technique.[27] Even though the mechanism of this enhancement is

not completely understood, it is accepted to be due to two major contributions: electromagnetic and chemical enhancement.[27,31] The electromagnetic contribution is wavelength dependant and arises from the collective oscillation of conduction electrons that occur when an electromagnetic wave, such as the incident radiation of a laser, interacts with a metals surface.[31] This effect contributes up to 10^{12} orders of magnitude of the signal. The chemical effect contributes far less to the enhancement, up to 10^2 orders of magnitude of the signal and arises due to a charge transfer between the metal surface and the adsorbate molecule.[31]

SERS can be coupled with electrochemical techniques to create electrochemical surface-enhance Raman spectroscopy (EC-SERS). This technique allows the detection of analyte molecules on a metallic surface at a chosen applied voltage. EC-SERS can be useful to detect signal of an analyte in biologically relevant environments and to monitor surface redox processes. Application of a voltage also changes the chemical environment and can change the position or conformation of the molecule on the surface. This technique can be exploited to get the desired position or confirmation of the analyte molecule while using the selective and sensitive SERS technique.[29]

3.3 Electrochemistry

Electrochemistry is a branch of physical chemistry that uses electrical energy to view and assess chemical changes. These chemical changes may arise due to the movement of charged species that occur in bulk solution by using electrical measurements of electrical quantities such as: current, potential, or charge. Applications of electrochemistry range from environmental monitoring, industrial quality control, and biomedical analysis.[32] Electrochemical measurements take place at the electrode-solution

interface, the two main types of electroanalytical measurements, potentiometric and potentiostatic.[32] Both potentiometric and potentiostatic methods require and electrochemical cell, which consists of electrodes (conductors) and an electrolytic solution.[32] The electrolyte is commonly an aqueous salt solution; however the choice of solvent depends on analytes redox and electrochemical activity, and the chemical reactivity of the solvent. The solvent should not react with the analyte, nor undergo electrochemical reactions over a wide potential range.[32] The concentration of the electrolyte customarily ranges from 0.1-1.0 M so as to have the electrolyte in large excess of all electroactive species. If there is oxygen present in the electrolyte, the reduction profile can interfere with the measurements of the analytes under investigation.[32] A common practice used in the removal of the undissolved oxygen is to purge the solution with an inert gas, such as nitrogen.

The focus of this research is on potentiostatic electrochemical techniques as they pertain to the following work. This technique can also be described as the controlled-potential technique as the electrode potential is being used to induce an electron-transfer reaction and the resultant current is measured.[32] Using the potentiostatic technique, the electrochemical cell contains three electrodes known as the working electrode (WE), the reference electrode (RE), and the counter electrode (CE). The WE is the electrode where the reaction takes place, while the RE has a stable and reproducible potential in which the WE is compared. The most commonly used REs are Ag/AgCl and Hg/Hg_2Cl_2 (saturated calomel electrode).[32] The CE is an inherent conducting material, commonly a platinum wire. During the application of an applied voltage, charged molecules will move closer or further away from the electrode surface, depending on their charge. Applying a potential

in the positive or negative direction can alter the charge of the WE surface and can thus attract oppositely charged molecules.[33]

When a substances surface is brought into contact with a polar medium, such as an aqueous solution, they will acquire a surface electric charge.[4,32] To compensate for this charge, nearby ions of opposite charge are attracted to the surface and those of like charge are repelled.[4,32] This formation is known as an electrical double layer and can be simply represented as shown in Figure 3.2.

Surface
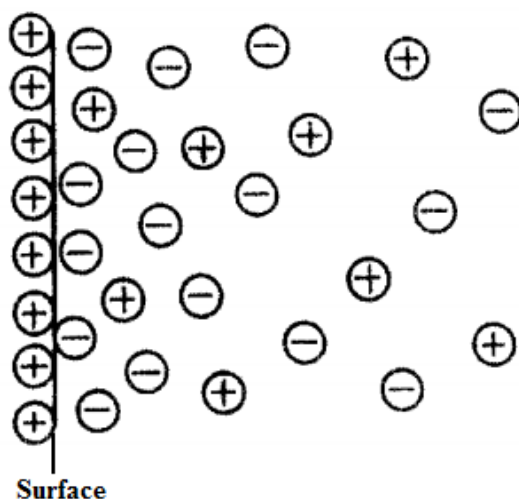
Figure 3.2: Simple illustration of the electrical double layer.[4]

The two layers of the electrical double layer are the compact and the diffuse layer. The compact layer contains both Helmoltz layers, the inner Helmoltz plane (IHP) and the outer Helmoltz plane (OHP). The IHP is the layer closest to the electrode and consists of solvent molecules and specifically adsorbed ions.[32,34] The OHP describes the imaginary plane passing through the center of solvated ions at their closest approach to the surface.[32] The compact layer refers to a compact layer of charges which are strongly held by the electrode and can survive even when the electrode is pulled from the solution, However, the Helmoltz model fails to take into consideration the thermal motion of ions

which would loosen then from such a compact layer.[32,34] The diffuse layer, or Gouy layer, is a three dimensional region of scattered ions which entends from the OHP to the bulk solution. The total charge of the compact and diffuse layers is equal and opposite to the net change of the electrode.[32,34]

Chapter 4: Materials and Methods

4.1 General

Gold (III) chloric hydrate (99.999%, HAuCl4), silver nitrate (99.9995%, AgNO3), 4-aminothiophenol (97%, C_6H_7NS), 2-aminothiophenol (99%, C_6H_7NS), 3-iodoaniline (98%, $IC_6H_4NH_2$), 2-iodoaniline (98%, $IC_6H_4NH_2$), sodium borohydride (99%, NaBH4), and sodium fluoride (99.99%, NaF) were all purchased from Sigma Aldrich (St. Louis, MO). 3-aminothiophenol (97%, C_6H_7NS) was purchased from Alfa Aesar (Ward Hill, MA). Glassware was immersed in an acid bath of 95-98% ACS grade sulfuric acid, or (for glassware used in AuNP) an aqua regia solution (HCl/HNO_3, 3:1) for several hours and rinsed thoroughly with ultra-pure water (>18.2 MΩ·cm) from a Milli-Q plus system (Millipore). The same Millipore water was used to prepare all solutions unless otherwise stated. Screen-printed carbon electrodes (SPEs) (15 x 61 x 0.36 mm) were purchased from Pine Research Instrumentation (Durham, North Carolina USA), and consisted of a silver/silver chloride (Ag/AgCl) RE, a carbon CE, and carbon WE (5 x 4 mm).

4.2 Nanoparticle Preparation and Characterization

4.2.1 Preparation of Silver Nanoparticles (AgNP)

Silver nanoparticles were prepared using a literature method.[35] This modification of the Lee-Meisel method mixes 1.0 mL of $AgNO_3$ solution (0.1M), 3.4 mL of aqueous sodium citrate (0.17 M), and 0.6 mL of citric acid (0.17 M) into a 250 mL three-necked flat bottom round flask (covered with tin foil to limit exposure to light) with 95 mL of water. 0.2 mL of freshly prepared sodium borohydride solution (0.1mM) was then added to this mixture while stirring. This solution was allowed to stir for one minute at room

temperature and is then brought to a boil under reflux within 20 minutes. After boiling for one hour, the silver nanoparticle colloidal sol was cooled to room temperature in air. The maximum absorption (extinction) peak of the colloidal silver nanoparticle suspension was ~392 nm, which is consistent with spherical silver nanoparticles.

4.2.2 Preparation of Gold Nanoparticles (AuNP)

Gold nanoparticles were prepared using a literature method.[35] This method combines 100.0 mL of aqueous $HAuCl_4$ (0.25 mM) into a 250 mL three-necked flat bottom round flask with 98.0 mL of water. This solution was then stirred and brought to a boil under reflux. Once boiling, 1.0 mL of aqueous 5% sodium citrate is added. The colloidal gold sol was then cooled to room temperature. The maximum absorption (extinction) peak of the colloidal gold nanoparticle suspension is ~520 nm, which is consistent with spherical gold nanoparticles.

4.2.3 Construction of Ag/AuNP Electrodes

The AgNP colloidal suspension was centrifuged at 8000 rpm for 20 minutes. The supernatant was then removed and discarded, and the pellet in each tube was collected together and centrifuged again at 8000 rpm for 20 min to obtain the silver concentrate (silver atom concentration of 0.4 M). The AuNP colloidal suspension obtained from above procedure was centrifuged in the same manner as above to obtain the gold concentrate. The SPEs were then functionalized by depositing three 5.0 μl layers of the concentrated nanoparticle suspension (AgNP or AuNP) onto the 5mm x4mm carbon WE using a micropipette. The electrodes were left to dry completely between the depositions of each layer, and the final layer was allowed to dry completely before the electrode was used.

4.3 Synthesis of 3,3'-DMAB and 2,2'-DMAB

To synthesize 3,3'-DMAB, 4.81 mL of 3-iodoaniline was then reacted with 9.2320 g of $NaBO_3 \cdot 4H_2O$ and 2.2266 g of H_3BO_3 in 100 mL of acetic acid at 55 °C for six hours while stirring. The reaction vessel was covered in tin foil to minimize the any photochemical reactions. The reaction was then left to cool to room temperature and gravity filtered to obtain the expected product of 3,3'-diiodoazobenzene. This product was then recrystallized in tetrahydrofuran (THF). The continuation of this reaction form 3,3'-diiodoazobenzene to 3,3'-DMAB was abandoned due to time constraints.

To synthesize 2,2'-DMAB, 2.2053 g of 2-iodoaniline was reacted with 1.5010 g of $NaBO_3 \cdot 4H_2O$ and 0.5512 g of H_3BO_3 in 100 mL of acetic acid at ~50°C for six hours while stirring. The reaction was then left to cool to room temperature and gravity filtered to obtain the expected product of 3,3'-diiodoazobenzene. This product was then recrystallized in tetrahydrofuran (THF). The continuation of this reaction form 2,2'-diiodoazobenzene to 2,2'-DMAB was abandoned due to time constraints.

4.4 Instrumentation

4.4.1 Raman Spectrometer

All spectral data for experiments were collected using a DXR Smart Raman spectrometer with a 180-degree sampling accessory manufactured by Thermo Fisher Scientific Inc. (Madison, WI, USA). The spectrometer is equipped with two different laser exication wavelengths (532 nm and 780 nm). The high-resolution grating has a range of 1800-50 cm^{-1}, with a spectral resolution of 3.0 cm^{-1}. The 532 and 780 nm lasers have power ranges of 1-10 and 10-150 mW, respectively. The spectrometer has a 10 μm laser spot size and is equipped with an air-cooled CCD detector. In these studies, Au/Ag

modified screen printed electrodes were used as substrates for Surface-Enhanced Raman Spectroscopy (SERS) and Electrochemical SERS (EC-SERS). All the spectra collected were analyzed using Origin 9.0 software (Northampton, MA, USA).

4.4.2 Potentiostat/Galvanostat

Electrochemical (EC) measurements for experiments were performed using a portable WaveNow USB Potentiostat/Galvanostat produced by Pine Research Instrumentation (Durham, NC, USA). The instrument connects to a standard computer, which uses software for setting electrochemical parameters. The electrochemical software, Aftermath Data Organizer (version 1.2.4361), is also produced by Pine Research Instrumentation. Electrochemical methods such as EC-SERS were performed using this USB potentiostat.

4.4.3 Electrochemical SERS Setup

The electrochemical SERS (EC-SERS) set up combines the Raman spectrometer and potentiostat described above. The Raman laser is focused onto the modified working electrode of the SPE in the electrochemical cell. The cell design consists of a standard disposable glass vial and a special mini USB adapter that is made to fit the SPEs. Raman spectra can then be collected at a desired applied potential. The potential was applied from 0.0 V to − 1.0 V at 0.1 V increments (cathodic direction). The potential was then returned from -1.0 V to 0.0 V (anodic direction) in the same increments. At each potential, a spectrum was collected for a time interval of 30 s. The supporting electrolyte used for EC-SERS was a deaerated 0.1M NaF solution. A diagram of the electrochemical SERS setup is shown in Figure 3.1.
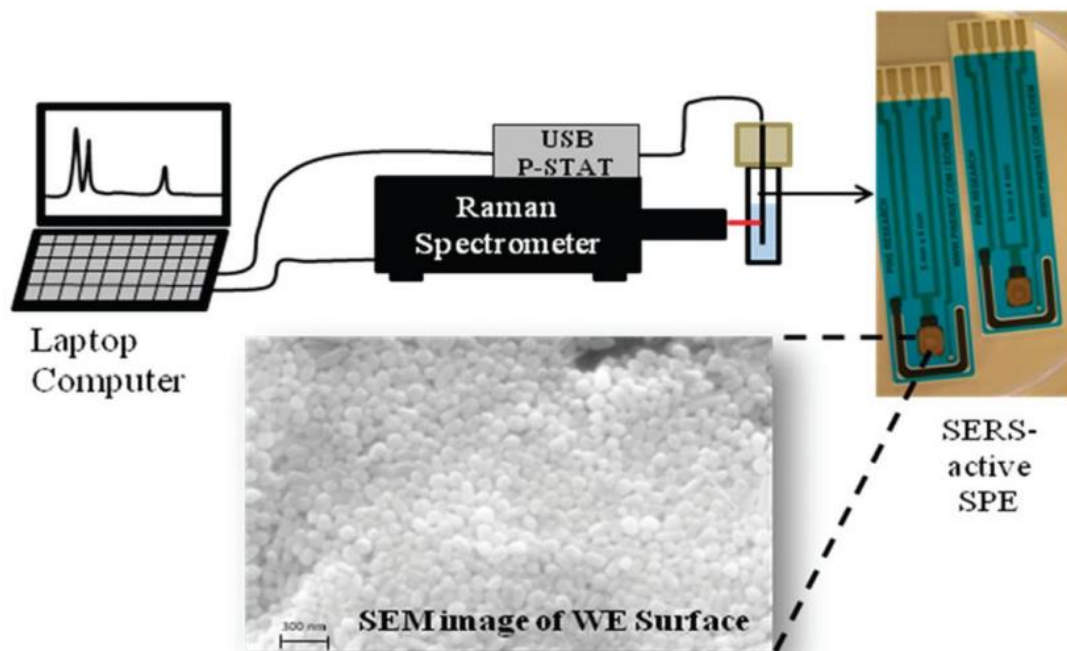
Figure 4.1: Schematic representation of the portable electrochemical surface-enhanced Raman setup. The inset shows an SEM image of the AgNP electrode surface.[36]

4.4.4 Cyclic Voltammetry (CV)

Cyclic Voltammetry (CV) was conducted at the end of each experiment to assess film quality and redox behavior of Raman reporters within the potential window of 0.0V to -1.0V, at a sweep rate of 50 mV/s.

4.4.5 Double Step Chronoamperometry (DPSCA)

Double step chronoamperometry (DPSCA) was conducted using the standard electrochemical cell setup, except using a solution of 1.0 mM 4-ATP in 0.1M NaF. In this study each cycle included an induction period during which 0V was held for 3 seconds, followed by a forward step of 0.4V which was held for 30 seconds, followed by a reverse step at -0.6V which was held for 30 seconds, after which a relaxation period of 0V was held for 3 seconds. DPSCA was employed to collect the 4,4'-DMAB oxidation product.

4.4.6 Signal Processing

Raman spectral data were processed using Origin 9 software, produced by OriginLab Corporation (Northampton, MA, USA). All spectra were normalized for both laser power and acquisition time for ease of data comparison, and also smoothed using adjacent averaging method with 9 points of window. CV data was also plotted using Origin 9 software. The data was copied from the electrochemical software (Aftermath) into Origin 9.

Chapter 5: Results and Discussion

5.1 4-Aminothiophenol (4-ATP) Studies

5.1.1 Normal Raman Spectroscopy

Initial studies were conducted using normal Raman spectroscopy for the pure powder form of 4-Aminothiophenol (4-ATP). Figure 5.1 shows the Raman spectrum of pure 4-ATP. This study is used to aid in the interpretation of the surface plasmon-assisted catalysis as a comparison tool once the molecule is place onto the nanoparticle functionalized SPE.
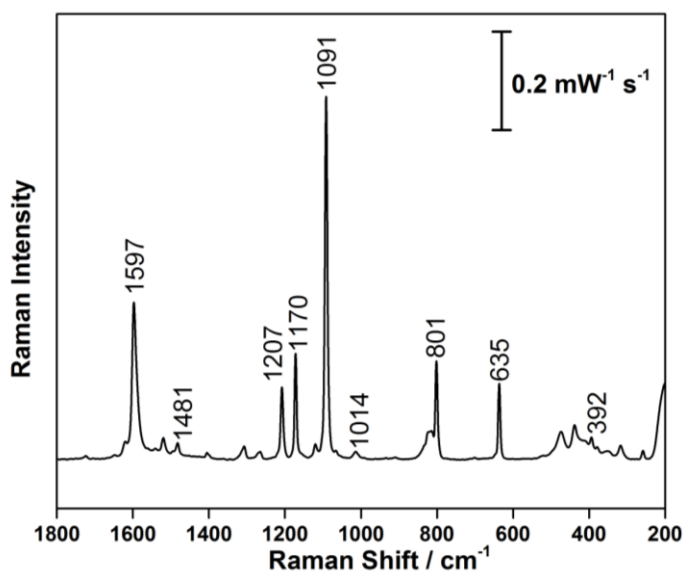
Figure 5.1: Raman spectra of pure 4-ATP powder. Measurement taken at 785nm, collected at 22.3 mW for a time interval of 30 seconds.

5.1.2 EC-SERS

Due to an inherent lack of sensitivity with normal Raman spectroscopy, the normal Raman spectra are generally not very useful for detection of analytes in solution at low concentration. For this reason, SERS was used to further study this analyte and others. A solution of 4-ATP with a concentration of 1.0 mM was prepared and drop

coated onto the functionalized electrode and allowed to air dry. A solution of 0.1 M NaF

was used as the supporting electrolyte in the electrochemical cell, as EC-SERS was used

to help characterize the behaviour of 4-ATP at the metal/solution interface. By looking at

Figures 5.2 and 5.3, it is apparent that there is a change in peaks due to the change in

voltage. This effect is most likely due to a change in the surface chemistry/charge of the

nanoparticle functionalized electrode, which occurs due to the application of a negative

voltage. Open circuit potential (OCP) is the resting potential for the metal and it is

measured without applying any potential. As a result, the OCP spectrum represents the

SERS signal generated in the absences of applied voltage.

Figure 5.2: SERS signal of 1 mM 4-ATP in 0.1 M NaF at OCP to -1.0V at intervals of -0.1V. Measurements taken on AuNP functionalized electrode at 780nm, collected at 80 mW for a time interval of 30 seconds.

By looking at the cathodic spectral data in Figure 5.2, it is apparent that by increasing the

negative voltage from 0V to -0.7V there is an increase in peak intensities. From -0.8V to

-1V a decrease can be seen. In the range of greater peak intensities, the peaks at

1144 cm^{-1}, 1391 cm^{-1} and 1439 cm^{-1} can be seen appearing and growing in intensity. At -0.8V these peakes can be seen to decrease again and are not observed at -1V. These peaks are associated with the 4,4'-DMAB molecule formed as a result of the plasmonic catalysis as shown in Table 5.1. A similar pattern of appearance and strengthening of intensities of the catalytic peaks and then their decrease again at -1V can be seen in Figures 5.3 and 5.4. These spectra show the similar analysis of 4-ATP but on AgNP and differ from each other due to the power and laser lines used.

Table 5.1: Peak assignments for 4-ATP (Raman) and 4,4'-DMAB (SERS, on silver substrates), the catalytic peaks are bolded.

Raman peaks/ cm^{-1}	SERS peaks/ cm^{-1}	Peak Assignment
392	387	ν(C-S)+ δ_{ip}(C-C)$_{Ar}$
-	**486**	**ν(C-S)**
635	642	ν(S-S)
-	**714**	**γ(C-C)$_{Ar}$**
801	816	$\delta_{ip,as}$ (C-C)$_{Ar}$
1014	1006	γ_{as}(C-H)
1091	1072	δ_{ip}(C-H)$_{Ar}$
-	**1143**	**$\delta_{ip,as}$(c-h)(ortho)**[b]
1170	1192	δ_{ip}(C-H)
1207	-	ν(N-N)+ $\delta_{ip,s}$(C-H)
-	**1391**	**ν_{as}(C-C)$_{Ar}$+$\delta_{ip,as}$(C-H)$_{Ar}$ + ν(N=N)**
-	**1440**	**$\delta_{ip,s}$(C-H)+ ν(N=N)**
1481	1472	δ_{ip}(C-C)$_{Ar}$+ $\delta_{ip,s}$(C-H) + ν(C-N)
1597	1577	ν(C=C)$_{Ar}$

[a]ν, stretching; δ, in plane bending; γ, out of plane bending; s, symmetrical; as, asymmetrical; ip, in-plane; Ar, aromatic ring
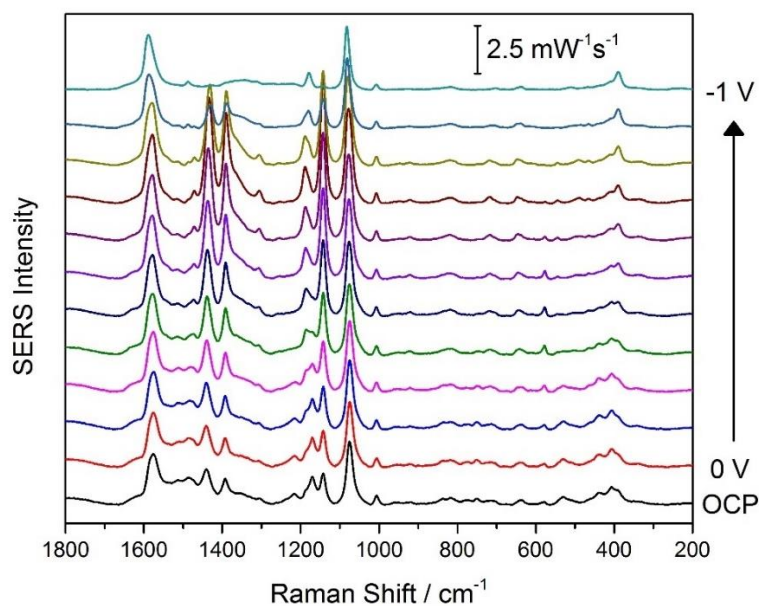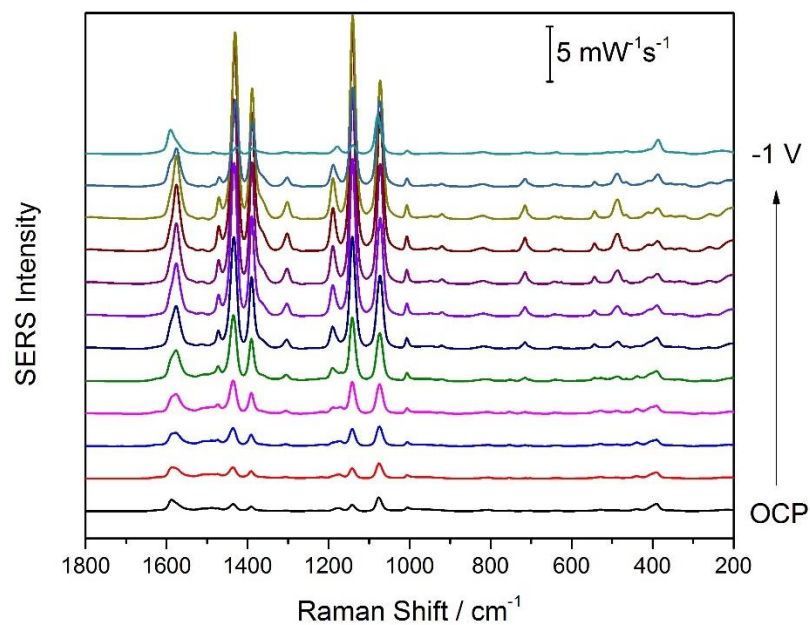
Figure 5.3: SERS signal of 1.0 mM 4-ATP in 0.1 M NaF at OCP to -1.0V at intervals of -0.1V. Measurements taken on AgNP functionalized electrode at 780 nm, collected at 80 mW for a time interval of 30 seconds.
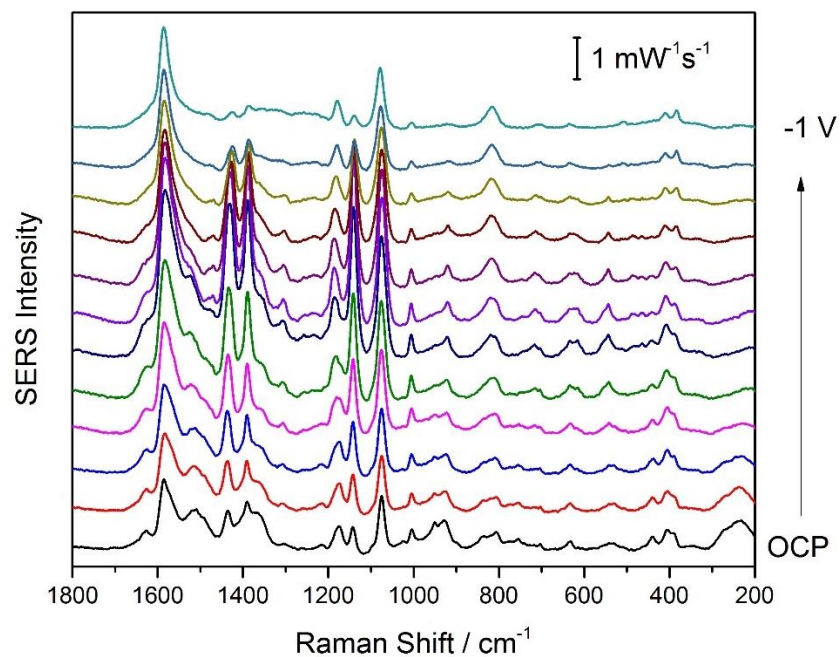
Figure 5.4: SERS signal of 1.0 mM 4-ATP in 0.1 M NaF at OCP to -1.0V at intervals of -0.1V. Measurements taken on AgNP functionalized electrode at 532 nm, collected at 3.0 mW for a time interval of 30 seconds.

When comparing the cathodic spectral data to the anodic data, as in Figure 5.5, the reversibility of the catalytic peaks and thus the catalytic ability can be seen. This spectrum not only shows the reversibility of the SPAC reaction, but shows electrochemistry as a useful technique to change the confirmation of molecules on the metal surface by changing the potential. The spectrum at OCP (cathodic) is purely due to the SPAC reaction, at -1V the spectrum is reduced ro the amine, and the final spectrum at 0V (anodic) is due both to electro oxidation and SPAC. The disappearance and reappearance of the catalytic peaks with the changing voltage as depicted in this spectrum is the main motivation of this project, seeing if this reaction works in other instances and the use of this reaction in industry or synthesis in the future.
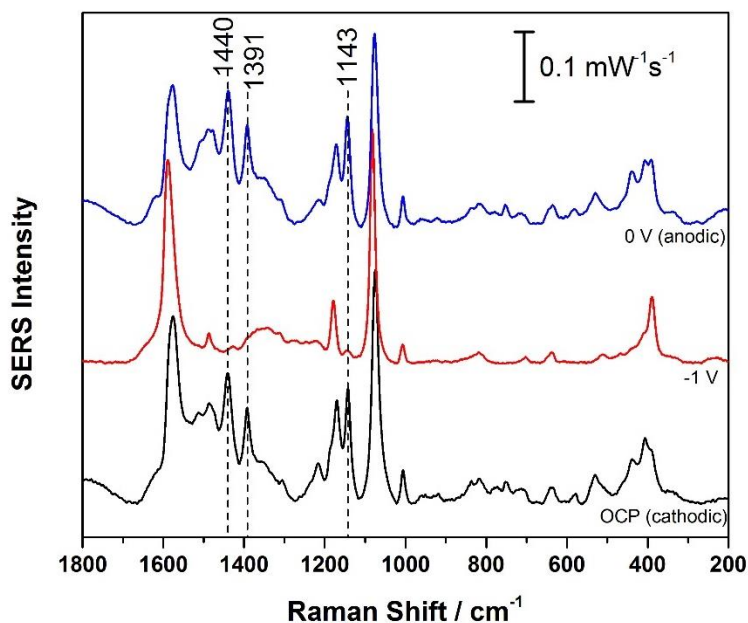
Figure 5.5: SERS signal of 1 mM 4-ATP at OCP to -1.0V (cathodic) and then back to 0V (anodic) at intervals of -0.1V. Measurements taken on AuNP functionalized electrode at 780 nm, collected at 80 mW for a time interval of 30 seconds. Catalytic peaks marked at 1143, 1391, and 1440 cm^{-1}.

5.2 3-Aminothiophenol (3-ATP) Studies

5.2.1 Normal Raman

As described above, the normal Raman spectrum is collected prior to the EC-SERS studies in order to provide a spectral comparison. As shown in Figure 5.6, the Raman spectrum is provided for pure 3-ATP. The peak assignments for this spectrum are shown in Table 5.2
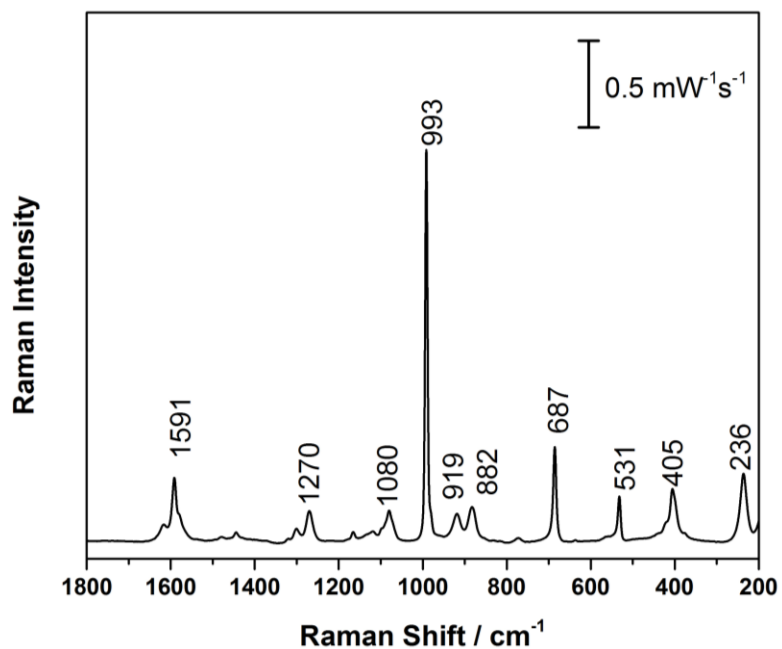
Figure 5.6: Normal Raman spectral data for 3-ATP at 780nm, collected at 80mW for 30 seconds.

Table 5.2: Peak assignments for the experimental Raman data for pure 3-ATP.

Experimental Raman peaks/ cm^{-1}	Peak Assignment
236	-
405	γ(C-C)+ν(C-S)
531	ω(NH$_2$)
882	ν(C-S)+β(S-H)
919	-
993	α(ring)
1083	δ_{as}(NH$_2$)
1077	ν(C-S)+β(C-H)
1270	ν(C-N)
1448	ν(C-C)
1591	ν(C-C)

ν, stretching; δ, bending; as, asymmetrical

5.2.2 EC-SERS

EC-SERS data was collected for 3-ATP to test if this molecule would react similarly to its isomer 4-ATP and exhibit SPAC. Spectra that either had changing peak intensities or new peaks appearing would be suggestive of the SPAC effect taking place, as shown with 4-ATP. As evident in Figures 5.7 and 5.8, the spectral data does not show significant change in peak intensities or positions with potential and resembles that of the normal Raman data obtained, and therefore 3-ATP does not show promise for exhibiting SPAC behaviour. This statement can be shown to hold true as Jiang et al. recently suggested the unlikelihood of 3-ATP performing this catalytic conversion due to

unfavourable radical cationic resonance structures.[5] The inability of the carbon attached to the sulfur atom to hold a positive charge while a radical is on the carbon atom attached to the nitrogen atom, as shown in Figure 5.9 (iv) for 4-ATP and (v) for 2-ATP, is why they explain that 3-ATP will not catalytically couple.[5] It is stated that because of the lack of this stable resonance structure, 3-ATP may not be stable enough to undergo the SPAC reaction. However, this resonance structure is available from 2-ATP so more promise was expected for that molecule.

Figure 5.7: SERS signal of 10 mM 3-ATP in 0.1 M NaF at OCP to -1.0V at intervals of -0.1V. Measurements taken on AgNP functionalized electrode at 780 nm, collected at 80 mW for a time interval of 30 seconds.

Figure 5.8: SERS signal of 10 mM 3-ATP in 0.1 M NaF at OCP to -1.0V at intervals of -0.1V. Measurements taken on AuNP functionalized electrode at 780 nm, collected at 80 mW for a time interval of 30 seconds.
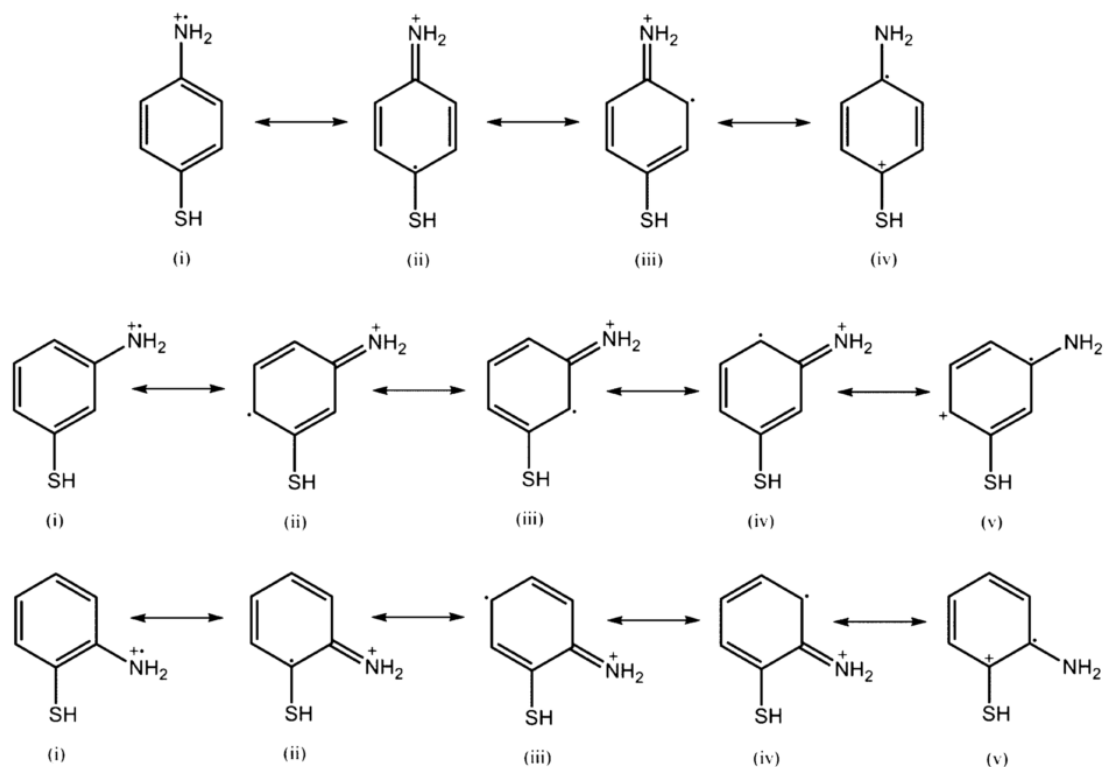
Figure 5.9: Resonance structures of the radical cations of 4-ATP, 3-ATP, and 2-ATP.[5]

5.3 2-Aminothiophenol (2-ATP) Studies

5.3.1 Normal Raman

As described above, the normal Raman spectrum is collected prior to the EC-SERS studies in order to have a spectral comparison. As shown in Figure 5.10, the Raman spectrum is provided for of pure 2-ATP. The peak assignments for this spectrum are shown in Table 5.3.
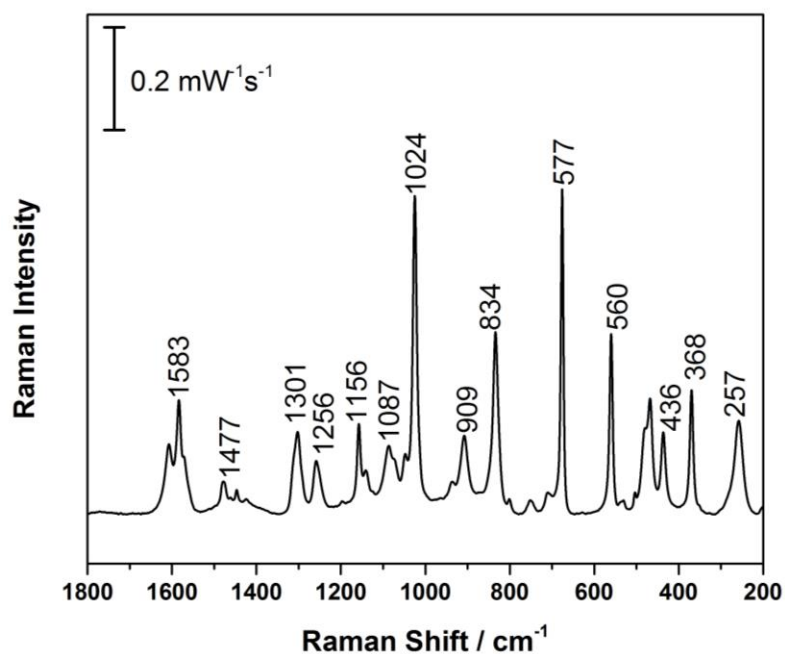
Figure 5.10: Normal Raman spectral data for 2-ATP at 780 nm, collected at 80mW for 30 seconds.

Table 5.3: Peak assignments for the experimental Raman data for pure 2-ATP.

Experimental Raman peaks/ cm^{-1}	Peak Assignment
436	γ(C-C)
560	-
577	-
834	-
909	δ(S-H)
1024	-
1087	δ_{as}(NH$_2$)
1156	-
1256	-
1301	ν(C-N)
1477	ν(C-C)
1583	ν(C-C)

ν, stretching; δ, bending; as, asymmetrical

5.3.2 EC-SERS

EC-SERS on 2-ATP was done to test if this molecule would exhibit SPAC similar to its isomer 4-ATP. Spectra that either had changing peak intensities or new peaks appearing would be suggestive of the SPAC effect also taking place, as shown with 4-ATP. As evident in Figures 5.11 and 5.12, the spectral data does not show much of a change in peak intensities or positions, however in both figures there is something changing at ~1450 cm^{-1}. This could possibly correspond to the oxidative product and therefore exhibits possible SPAC behaviour.
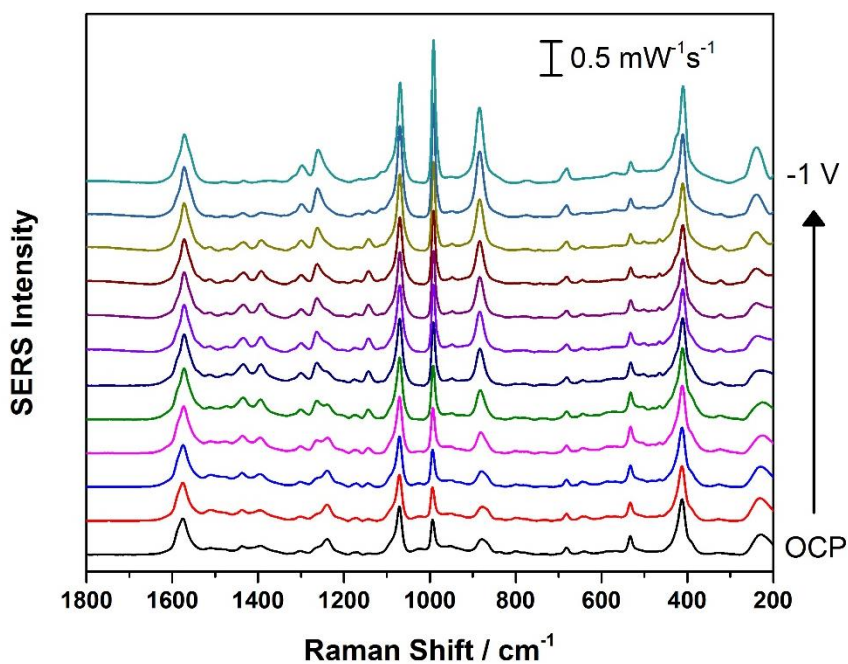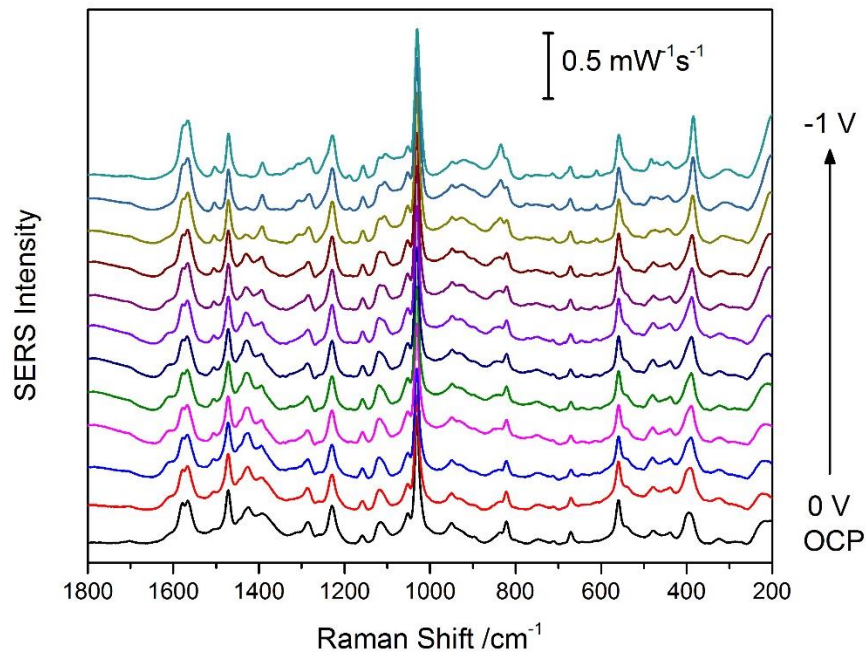
Figure 5.11: SERS signal of 10 mM 2-ATP in 0.1 M NaF at OCP to -1.0V at intervals of -0.1V. Measurements taken on AgNP functionalized electrode at 780 nm, collected at 80 mW for a time interval of 30 seconds.
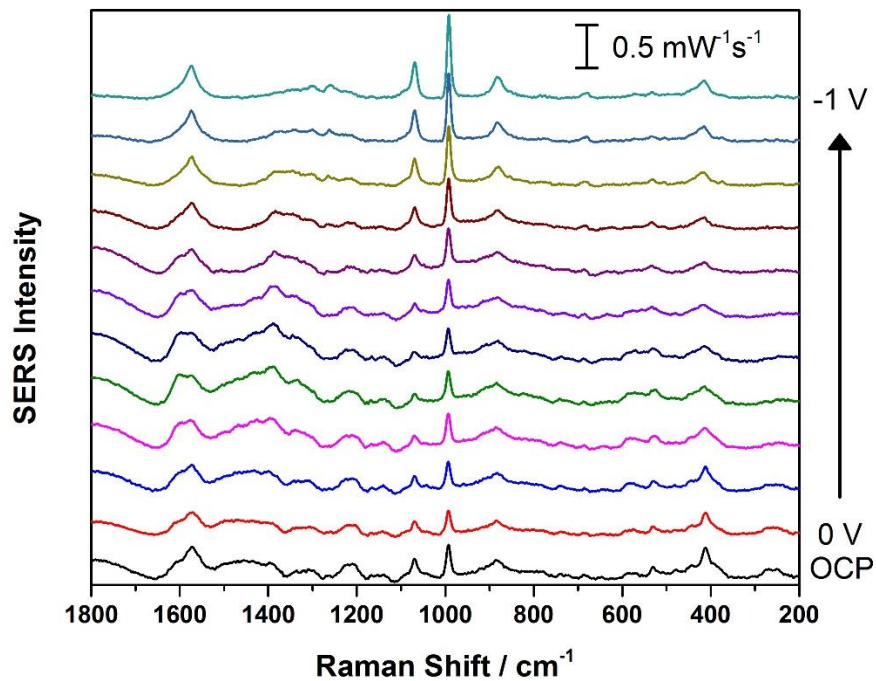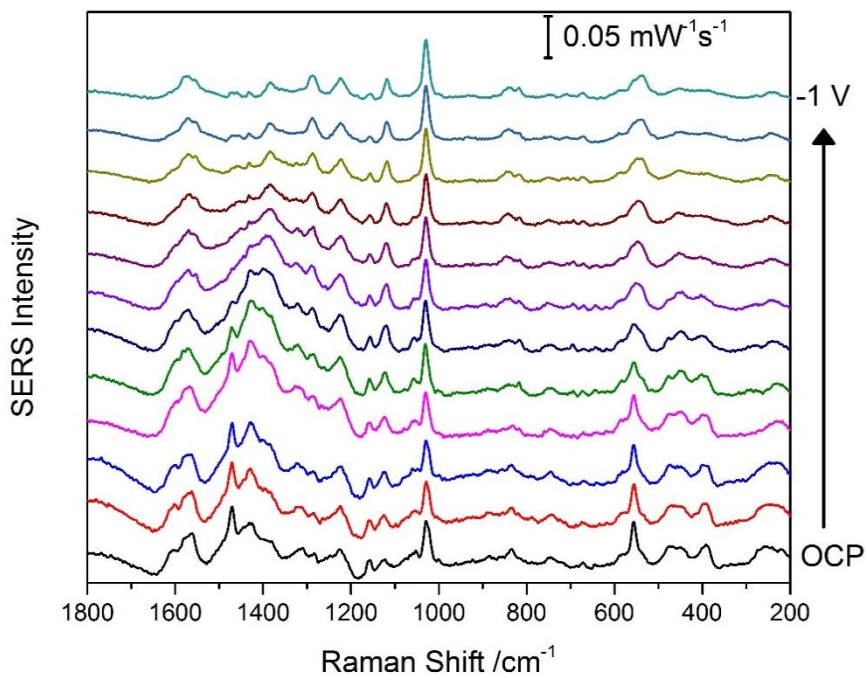

Figure 5.12: SERS signal of 10 mM 2-ATP in 0.1 M NaF at OCP to -1.0V at intervals of -0.1V. Measurements taken on AuNP functionalized electrode at 780 nm, collected at 80 mW for a time interval of 30 seconds.

5.4 3,3'-DMAB and 2,2'-DMAB

5.4.1 Synthesis of 3,3'-DMAB and 2,2'-DMAB

The synthesis of 3,3'-DMAB and 2,2'-DMAB were attempted to compare to the SERS data for the ATP analogues to examine if the SPAC reaction had indeed occurred. The synthesis followed the procedure as outlined in Huang et al., except starting with the x-iodoaniline complex instead of aniline.[3] Figure 5.13 shows the ^{1}H NMR spectrum of the starting material (3-iodoaniline) for the synthesis of 3,3'-DMAB. This spectrum shows the four aromatic hydrogens in the peaks labeled B, C, and D, and the amine hydrogens labelled A. The peak labelled E is the residual solvent peak of CD_2Cl_2.[37]
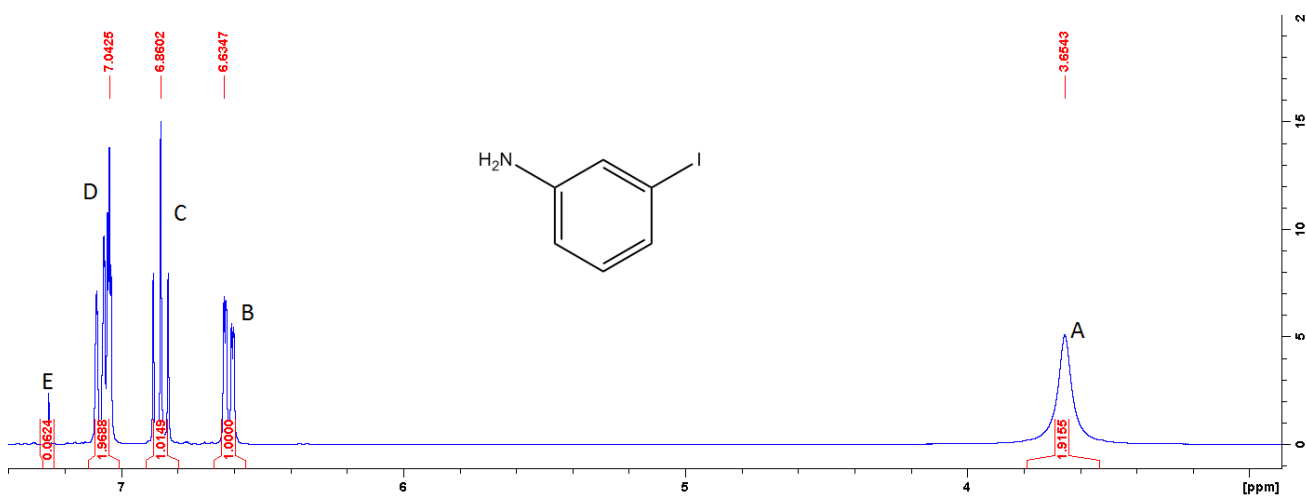
Figure 5.13: ^{1}H NMR spectrum of 3-iodoaniline in CD_2Cl_2

The first step of the reaction procedure was to form the diiodoazobenzene complex. When looking at the NMR spectrum of the recrystallized product, Figure 5.14, double the number of expected peaks are observed. The peaks labelled C are the aromatic peaks which integrate to six, the additional two peaks are labelled A, these integrate to more than two as they include the residual solvent peaks. The peaks labelled B are impurities present in the sample, more impurity peaks can be seen further downfield in

37

the spectrum, but are cut out from Figure 5.14 to better show the aromatic region. With the similar patterns of the peaks, and the exact double the expected amount, it can be realized that two isomers are present in this sample, the cis and trans isomers. This is justified when a COSY spectrum was obtained Figure A.1, showing two groups of coupling peaks.
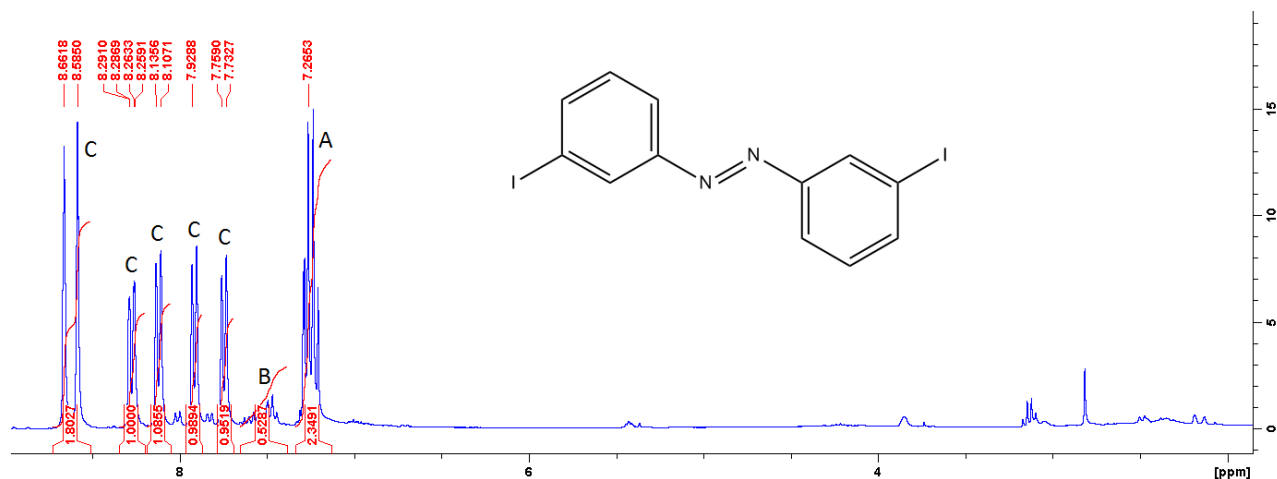
Figure 5.14: ^{1}H NMR spectrum of the synthesized product in CD$_2$Cl$_2$

To separate the cis and trans isomers and move forward with the synthesis of the DMAB product, column chromatography was used. When added to the column in a solvent mixture of 9:1, hexanes:chloroform, two products were obtained. Figure 5.15 shows the ^{1}H NMR spectrum of the separated isomer; however by this method alone the exact isomer could not be determined. Peaks labelled B show the aromatic hydrogens, which integrates to three, the additional aromatic hydrogen peaks is labelled A and integrates to more than one as the residual solvent peak of CD$_2$Cl$_2$ is also present.
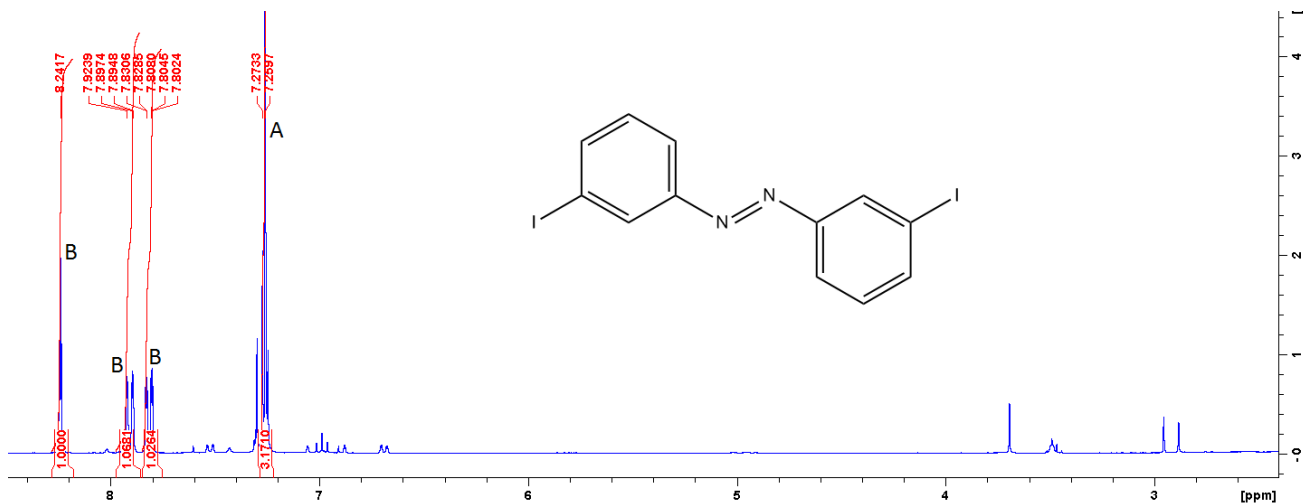
Figure 5.15: ^{1}H NMR spectrum of the separated product in CD$_2$Cl$_2$

The next step in the reaction procedure was to perform a Grignard reaction and replace the iodine atom with sulfur. However, this step was abandoned due to time constraints and computational methods were otherwise explored.

A similar reaction as described above was performed with 2-iodoaniline with the goal of synthesizing the molecule 2,2'-DMAB. Figure 5.16 shows the ^{1}H NMR spectrum of the starting material 2-iodoaniline. The aromatic hydrogen peaks are labelled B, C, D, and E, whereas the amide hydrogen peaks are labelled A. Finally, the residual solvent peak of CD$_2$Cl$_2$ is labelled F.
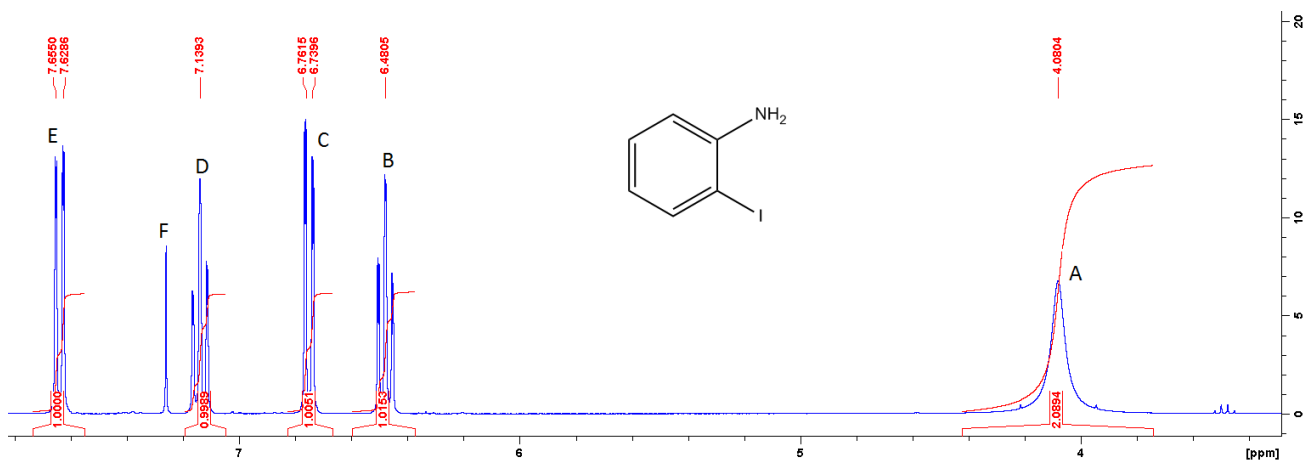
Figure 5.16: ^{1}H NMR spectrum of 3-iodoaniline in CD$_2$Cl$_2$

Again, the first step in the reaction was to create the diiodoazobenzene analogue. This reaction was preformed and the crude NMR spectrum is shown as the bottom line in Figure 5.17. This spectrum is compared to the starting material spectrum and shows that the product is mostly starting material, however contains some product, shown by the additional aromatic peaks similar to that of 3,3'-diiodoazobenzene product above.
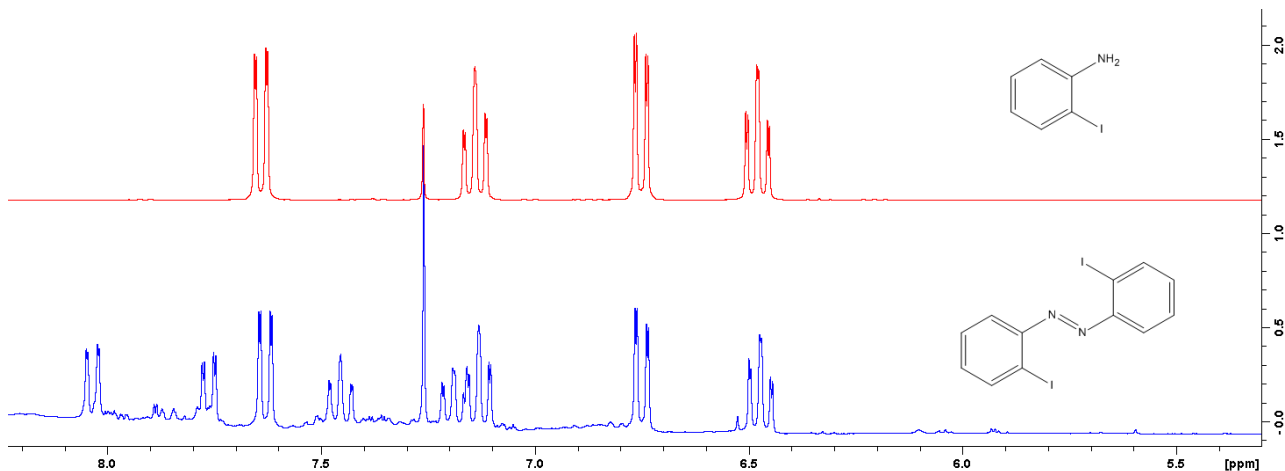
Figure 5.17: Comparison of the ^{1}H NMR spectra of 2-iodoaniline (top) and the crude, synthesized product believed to be 2,2'-diiodoazobenzene (bottom).

Again, efforts to further synthesize the desired product were abandoned due to time constraints and computational methods explored.

5.4.2 Calculated 3,3'-DMAB and 2,2'-DMAB Raman spectra

Since efforts to synthesize the DMAB products had to be abandoned, DFT calculations were provided by Yaoting Zhang for 3,3'-DMAB and 2,2'-DMAB Raman spectra. These calculated spectra where then compared to the EC-SERS data in the above section. It can be seen in Figure 5.18 that the experimental EC-SERS data of 3-ATP does not correspond with the calculated spectra of 3,3'-DMAB, therefore, it can be said that

under these conditions 3-ATP does not go through the SPAC conversion. The peak assignments of both cases are shown in Table A.1
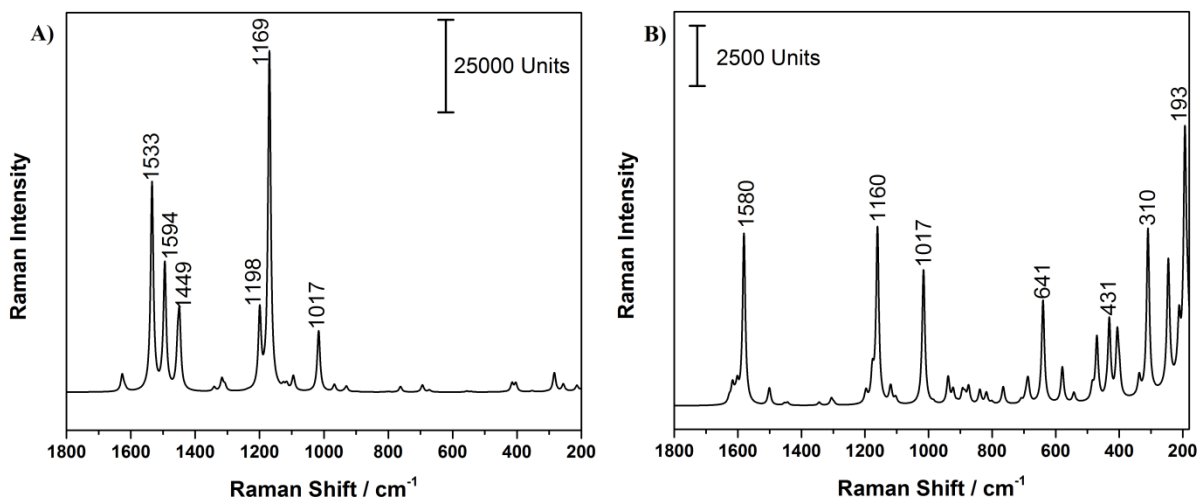
Figure 5.18: DFT calculated Raman spectra of (A) trans-3,3'-DMAB at 780 nm and (B) cis-3,3'-DMAB at 780 nm.

Again, the data from the experimental EC-SERS of 2-ATP was further compared to DFT calculations for the SPAC product 2,2'-DMAB. It can be seen in Figure 5.19 that the experimental EC-SERS data does not correspond with the computational spectra of 2,2'-DMAB and rather resembles more that of the normal Raman spectrum of 2-ATP. The anomaly at ~1450cm^{-1} from the experimental data (Figures 5.11 and 5.12) could possibly compare to 1446cm^{-1} peak in the trans-2,2'-DMAB calculated spectrum. However, these two spectra cannot be directly comparable due to their difference in techniques, but it can be said that under these conditions 2-ATP is more probable to SPAC conversion than 3-ATP. Nevertheless, since the experiment SERS spectra resemble more the normal Raman of pure 2-ATP it is unlikely that this is not the case. Peak assignments for both cases are shown in Table A.2.
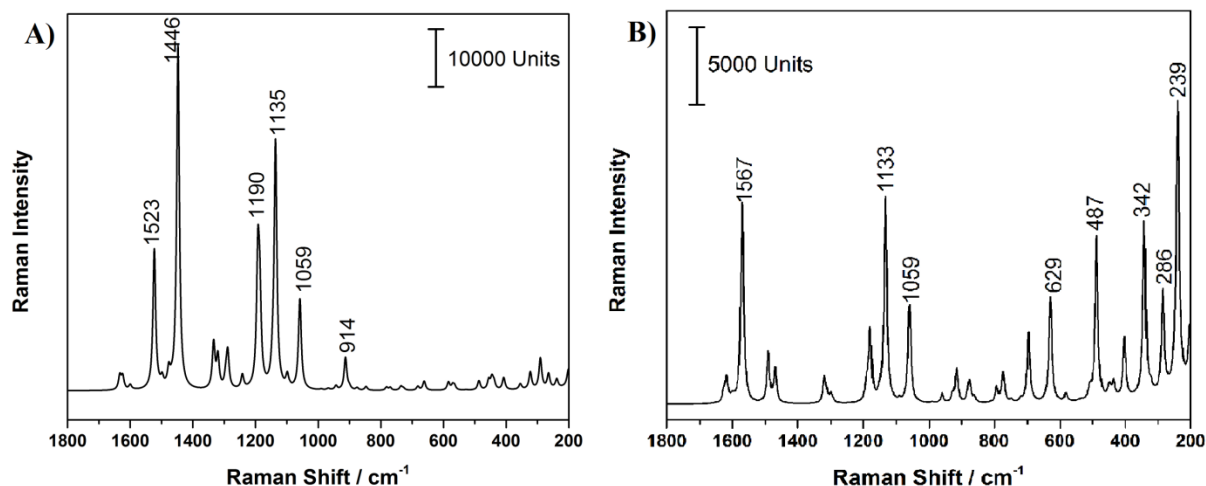
Figure 5.19: DFT calculated Raman spectra of (A) trans-2,2'-DMAB at 780 nm and (B) cis-2,2'-DMAB at 780 nm.

Both 3-ATP and 2-ATP did not undergo the SPAC conversion to their DMAB constituents as did the molecule 4-ATP. Thus it can be said that the substitution pattern on the benzene ring plays a big role in the SPAC conversion and only the para disubstituted pattern affords a SPAC product. Even though the reaction is not ubiquitous as was thought when entering this project, it may be useful for other purposes such as solid state synthesis.

5.5 Electrochemical Anodic Desorption of Aminothiophenol Molecules

One of the primary concerns in catalysis is the reusability of the catalyst. To exhibit this, the molecule of interest must be able to be removed from the catalyst surface, and the catalyst must be unchanged and therefore reusable. To demonstrate the reusability of the catalyst in this case, the aminothiophenol molecule was dropcoated onto an AuNP functionalized electrode and the potential increased positively until the molecule desorbed from the surface, otherwise known as anodic desorption. Going in the positive direction insures that the molecule on the surface is transformed into the DMAB product and that will be the molecule that is desorbed. Since positive voltages are

required for anodic desorption, only Au modified electrodes could be used for these studies due to the tendency of Ag to oxidize at positive applied voltages.

Figure 5.20 shows the anodic desorption of 4,4'-DMAB from the surface. To ensure the molecule was desorbed and there was no destruction of the catalyst, Figure 5.21 shows the reapplication of 4-ATP and the reusability of the electrode for SERS measurements and SPAC.

Figure 5.20: SERS signal of 1 mM 4-ATP in 0.1 M NaF at OCP to +1.0V at intervals of +0.1V. Measurements taken on AuNP functionalized electrode at 780 nm, collected at 80 mW for a time interval of 30 seconds.
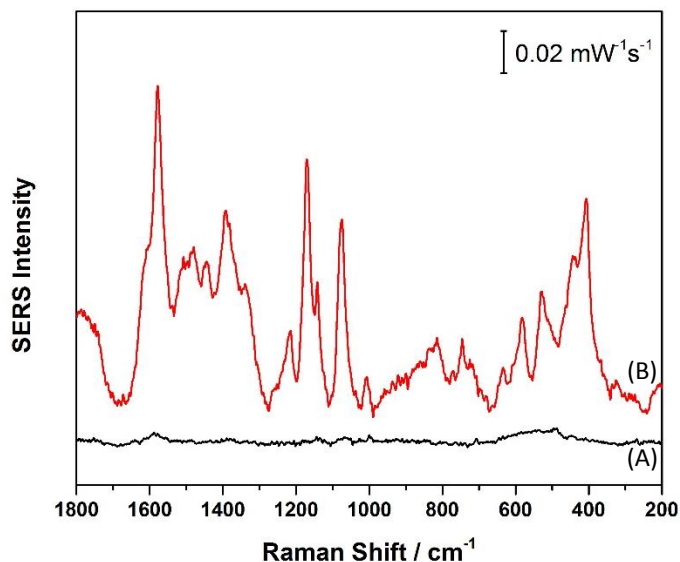
Figure 5.21: SERS signal of (A) desorption of 4-ATP/4,4'-DMAB and (B) the reapplication of 1mM 4-ATP. Measurements taken on AuNP functionalized electrode at 780 nm, collected at 80 mW for a time of 30 seconds.

3-ATP is also able to be anodically desorbed from the electrodes surface, however, since there is no evidence that it undergoes the SPAC conversion, it comes off the surface as 3-ATP and not the DMAB product as in 4-ATP. Conflictingly, 2-ATP does not act in a similar fashion and is not able to be desorbed from the surface. A reasoning behind the different reactivity of 2-ATP is the position of the substituent in relation to the sulfur group on the benzene ring. It is known that sulfur bonds strongly to gold, but so does nitrogen. It is believed that in the adsorption of 2-ATP to the gold nanoparticle not only does sulfur bond, nitrogen is also able to bond due to its close proximity to the gold in relation to the molecules 3-ATP and 4-ATP. Due to this stronger affinity to the gold surface, 2-ATP is not able to go through anodic desorption. These studies can be found in Figures 5.22, and 5.23 for 3-ATP and 2-ATP, respectively.
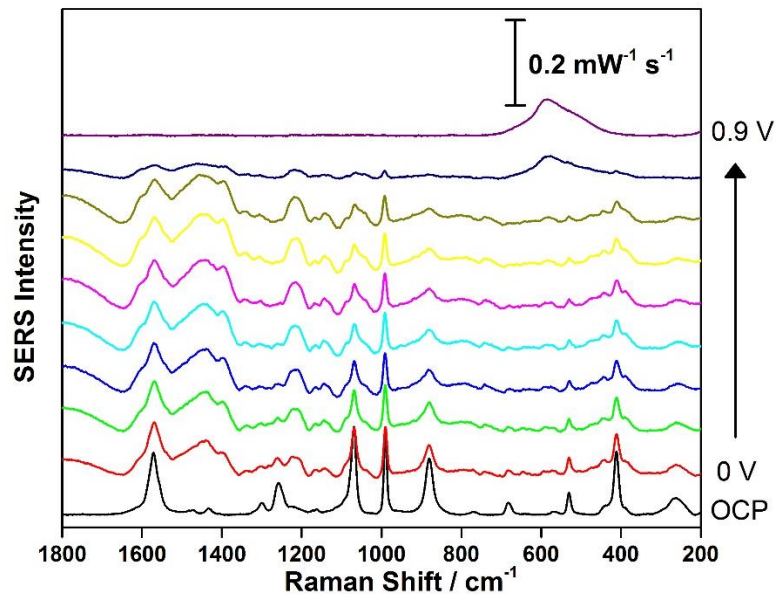
Figure 5.22: SERS signal of 10 mM 3-ATP in 0.1 M NaF at OCP to +0.9V at intervals of +0.1V. Measurements taken on AuNP functionalized electrode at 780 nm, collected at 80 mW for a time interval of 30 seconds.
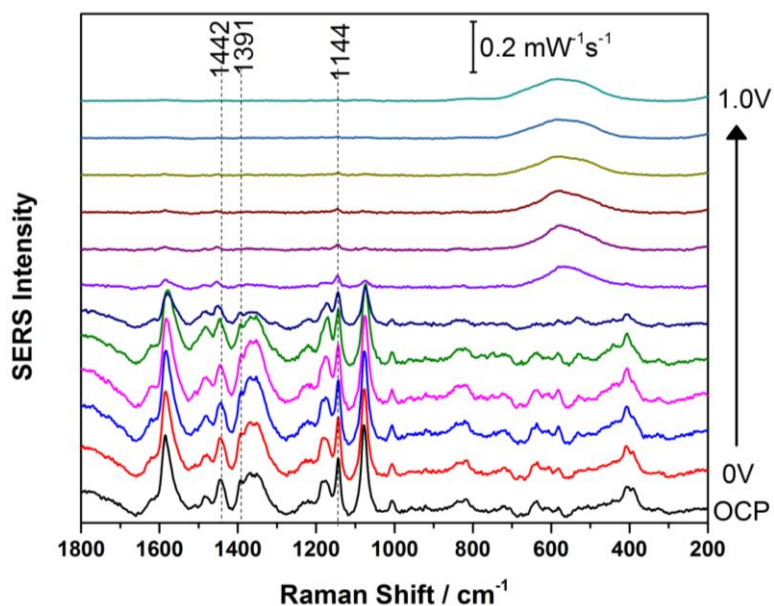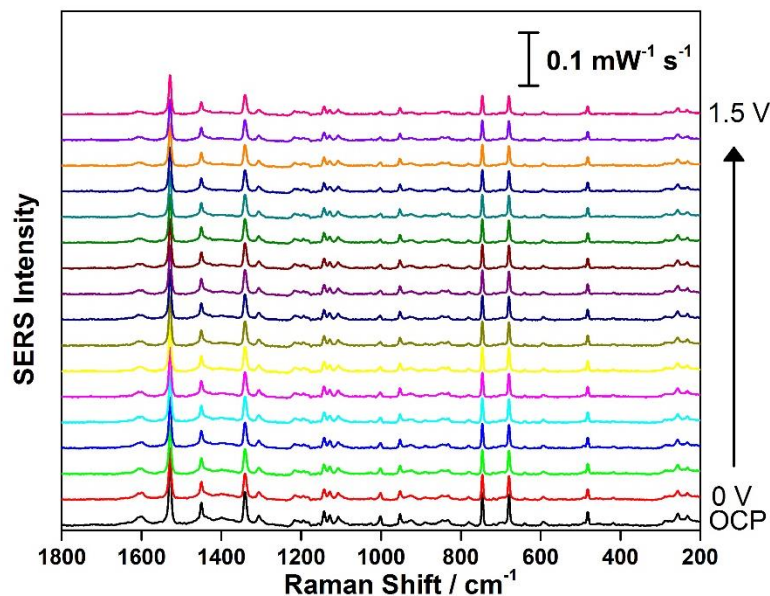

Figure 5.23: SERS signal of 10 mM 2-ATP in 0.1 M NaF at OCP to +1.5V at intervals of +0.1V. Measurements taken on AuNP functionalized electrode at 780 nm, collected at 80 mW for a time interval of 30 seconds.

To ensure that the molecule being desorbed from the surface was in fact the DMAB product in the case of 4-ATP, double step chronoamperometry (DPSCA)

electrochemical studies were performed. In this case the voltage had a forward step potential of 0.4V which lasted for 30 seconds and then had a reverse step potential at -0.6V which also lasted for 30 seconds, this allowed 4-ATP to be adsorbed, oxidized to 4,4'-DMAB, and then desorbed. After 130 cycles of this stepping action, a yellow solid could be seen to form on the surface of the working electrode. Figure 5.24 shows the Raman spectrum collected from this solid and confirms the identity to be 4,4'-DMAB.
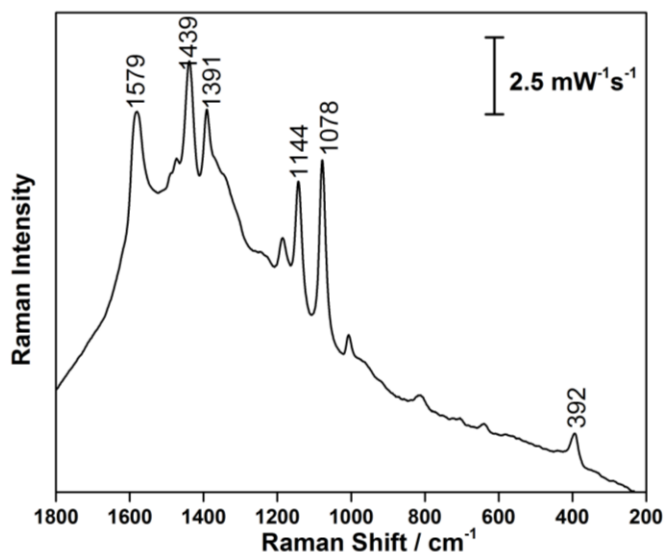
Figure 5.24: Normal Raman of the product formed from DPSCA at 785 nm, collected at 55.9 mW for 30 seconds.

5.6 4-Aminothiophenol (4-ATP) as a Probe Molecule

4-Aminothiophenol is a commonly used probe molecule in Raman spectroscopy and SERS. As shown in previous work and again in this work, 4-ATP goes through SPAC conversion and changes its orientation on the metal surface and thus changes the spectra obtained from this catalytic procedure. 4-ATP is currently being used as the probe molecule and a standard in many studies, some being quantitative biological tests.[38–40] However, with the catalytic abilities of this molecule, it could be questioned if this probe

molecule should be held at such a high standard, or if one with similar characteristics and affinity to gold but does not go through this conformational and spectral change should be used. When comparing 4-ATP, 3-ATP, and 2-ATP on AuNP functionalized electrodes in air (Figure 5.25) and at OCP (Figure 5.26) it can be seen that 2-ATP has similar intensity as 4-ATP and could be used as an alternative to have a good probe molecule but without the worry of its changing configuration on the surface.
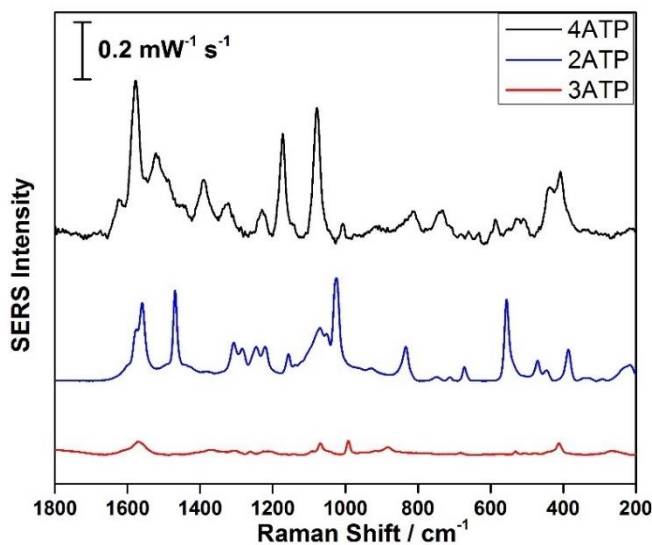
Figure 5.25: Raman signal of 1 mM 4-ATP, 10 mM 3-ATP, and 10 mM 2-ATP in air. Measurements taken on AuNP functionalized electrode at 780 nm, collected at 80 mW for a time interval of 30 seconds.
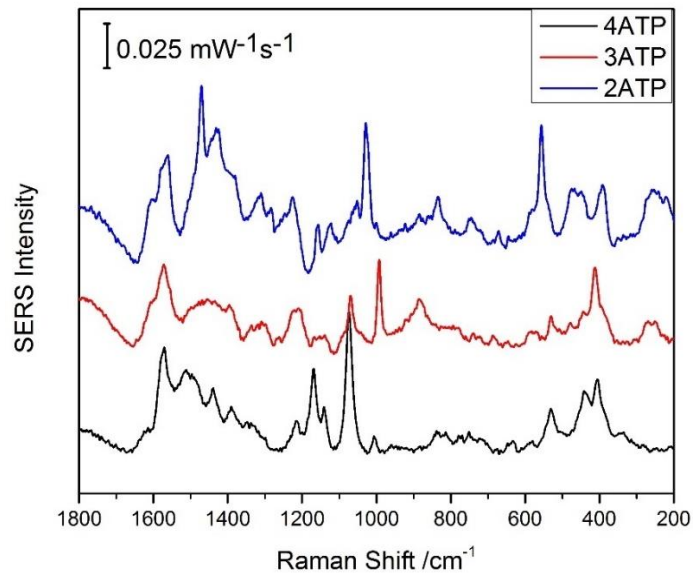
Figure 5.26: SERS signal of 1 mM 4-ATP, 10 mM 3-ATP, and 10 mM 2-ATP at OCP in 0.1 M NaF. Measurements taken on AuNP functionalized electrode at 780 nm, collected at 80 mW for a time interval of 30 seconds.

**Chapter 6: Conclusions and Future Work**

6.1 Conclusions

The surface plasmon assisted catalysis abilities of aminothiophenol derivatives were investigated through electrochemical surface enhanced Raman spectroscopy. SERS and EC-SERS were successfully used to characterize 4-ATP, 3-ATP, and 2-ATP on both gold and silver nanoparticle surfaces. Using these techniques, it was possible to comment on the SPAC abilities in reference to the conversion of 4-ATP to 4,4'-DMAB. Both 3-ATP and 2-ATP did not catalytically behave as 4-ATP under the same conditions, allowing it to be said that the position of the substituents on the benzene ring are important to the surface plasmon catalytic process.

The anodic desorption method for stripping the molecule off of the surface of the electrode worked as expected for 4-ATP and 3-ATP. However, with 2-ATP the molecule was not able to be removed from the surface, showing that the ortho situated amine group could also bind to the metal surface due to the close proximity. Also, using this method of anodic desorption, 4,4'-DMAB was able to be electrochemically formed on the surface of the WE and then stripped off. This product was able to be isolated and collected, exhibiting the potential use of the SPAC reaction as a new route for heterogeneous catalysis and electrochemical routes for generating new molecules.

Due to the SPAC conversion, 4-ATP may not be the most applicable probe molecule when doing quantitative tests. Isomers, 2-ATP and 3-ATP were compared to 4-ATP in air and at OCP to see if a similar molecule without the known SPAC conversion could be a viable replacement. 2-ATP had similar intensity as 4-ATP and could possibly

be used as an alternative probe molecule but without the worry of its changing configuration on the surface.

6.2 Future Work

Future work would entail the testing of the SPAC abilities on other thiol molecules such as thiophene and benzothiophene. These molecules are common in crude bitumen, therefore if the SPAC conversion was able to work on sulfur heterocycles there would be a way to selectively, and catalytically desulfinate the bitumen. These molecules could then later be stripped from the surface of the electrode and reused or disposed of correctly without the current waste of how sulfur containing molecules are removed from crude bitumen presently.

Since it was determined that the SPAC ability is dependent on the substitution pattern of the analytes, it would be worthwhile to test other para substituted thiols. Since the two know SPAC conversions to the oxidative product of 4,4'-DMAB are of para substituted ATP and NBT it would be expected that other para substituted thiols would react similarly.

During the SPAC formation of 4,4'-DMAB, the molecule is confined to the surface, but research has shown its confirmation can be reversibly switched on metal surfaces by using electric field, a scanning tunneling microscope tip, or light.[41,42,43] However, during our EC-SERS process it is most probable to be in the trans-confirmation.[41] This could allow for the possible investigation into synthesis where something could be added across the nitrogen-nitrogen double bond while held in trans-confirmation

References

(1)   Rycenga, M.; Cobley, C. M.; Zeng, J.; Li, W.; Moran, C. H.; Zhang, Q.; Qin, D.; Xia, Y. Controlling the Synthesis and Assembly of Silver Nanostructures for Plasmonic Applications. *Chem. Rev.* **2011**, *111* (6), 3669–3712.

(2)   Dong, B.; Fang, Y.; Chen, X.; Xu, H.; Sun, M. Substrate-, Wavelength-, and Time-Dependent Plasmon-Assisted Surface Catalysis Reaction of 4-Nitrobenzenethiol Dimerizing to p,p'-Dimercaptoazobenzene on Au , Ag , and Cu Films. *Langmuir* **2011**, *27*, 10677–10682.

(3)   Huang, Y. F.; Zhu, H. P.; Liu, G. K.; Wu, D. Y.; Ren, B.; Tian, Z. Q. When the Signal Is Not from the Original Molecule to Be Detected: Chemical Transformation of Para-Aminothiophenol on Ag during the SERS Measurement. *J. Am. Chem. Soc.* **2010**, *132* (27), 9244–9246.

(4)   Shaw, D. J. *Introduction to Colloid and Surface Chemistry*, 4th ed.; Elsevier Science Ltd.: Burlington, 1992.

(5)   Jiang, R.; Zhang, M.; Qian, S. L.; Yan, F.; Pei, L. Q.; Jin, S.; Zhao, L. Bin; Wu, D. Y.; Tian, Z. Q. Photoinduced Surface Catalytic Coupling Reactions of Aminothiophenol Derivatives Investigated by SERS and DFT. *J. Phys. Chem. C* **2016**, *120* (30), 16427–16436.

(6)   Huang, Y.; Dong, B. PH Dependent Plasmon-Driven Surface-Catalysis Reactions of P,p'-dimercaptoazobenzene Produced from Para-Aminothiophenol and 4-Nitrobenzenethiol. *Sci. China Chem.* **2012**, *55* (12), 2567–2572.

(7)   George, S. M. Heterogeneous Catalysis: Introduction. *Chem. Rev.* **1995**, *95* (3), 477–476.

(8)   Atkins, P.; de Paula, J.; Friedman, R. *Physical Chemistry: Quanta, Matter, and Change*, 2nd ed.; Oxford University Press: Oxford, 2009.

(9)   Modak, J. M. Haber Process for Ammonia Synthesis Jayant M Modak. *Resonance* **2002**, *7* (8), 69–77.

(10)   Rothenberg, G. *Catalysis: Concepts and Green Applications*; Wiley-VCH: Weinheim, 2008.

(11)   David, M.E.; Davis, R. J. *Fundamentals of Chemical Reaction Engineering*; McGraw-Hill Higher Education: New York, 2003.

(12)   Moshfegh, A. Z. Nanoparticle Catalysts. *J. Phys. D* **2009**, *42* (23), 233001.

(13)   Pushkarev, V. V.; Zhu, Z.; An, K.; Hervier, A.; Somorjai, G. A. Monodisperse Metal Nanoparticle Catalysts: Synthesis, Characterizations, and Molecular Studies under Reaction Conditions. *Top. Catal.* **2012**, *55* (19–20), 1257–1275.

(14)   Jambovane, S. R.; Nune, S. K.; Kelly, R. T.; Mcgrail, B. P.; Wang, Z.; Nandasiri, M. I.; Katipamula, S.; Trader, C.; Schaef, H. T. Continuous , One-Pot Synthesis and Post-Synthetic Modification of NanoMOFs Using Droplet Nanoreactors. *Nat. Publ. Gr.* **2016**, No. October, 1–9.

(15)   Huang, C.; Wang, H.; Wang, X.; Gao, K.; Wu, J.; Hou, H.; Fan, Y. Surfactant-Assisted Nanocrystalline Zinc Coordination Polymers: Controlled Particle Sizes and Synergistic Effects in Catalysis. *Chem. - A Eur. J.* **2016**, *22* (18), 6389–6396.

(16)   Anderson, S. R.; Mohammadtaheri, M.; Kumar, D.; O'Mullane, A. P.; Field, M. R.; Ramanathan, R.; Bansal, V. Robust Nanostructured Silver and Copper Fabrics with Localized Surface Plasmon Resonance Property for Effective Visible Light Induced Reductive Catalysis. *Adv. Mater. Interfaces* **2016**, *3* (6), 1500632.

(17) Willets, K. A.; Duyne, R. P. Van. Localized Surface Plasmon Resonance Spectroscopy and Sensing. *Annu. Rev. Phys. Chem.* **2007**, *58*, 267–297.

(18) Sun, M. Nanoparticle Catalysis by Surface Plasmon. In *New and Future Developments in Catalysis: Catalysis by Nanoparticles*; Suib, S. L., Ed.; Elsevier: Amsterdam, 2013; pp 473–487.

(19) Kang, L.; Xu, P.; Zhang, B.; Tsai, H.; Han, X.; Wang, H.-L. Laser Wavelength- and Power-Dependent Plasmon-Driven Chemical Reactions Monitored Using Single Particle Surface Enhanced Raman Spectroscopy. *Chem. Commun.* **2013**, *49* (33), 3389.

(20) Osawa, M.; Matsuda, N.; Yoshii, K.; Uchida, I. Charge-Transfer Resonance Raman Process in Surface-Enhanced Raman-Scattering From P-Aminothiophenol Adsorbed on Silver - Herzberg-Teller Contribution. *J. Phys. Chem.* **1994**, *98* (48), 12702–12707.

(21) Wu, D. Y.; Liu, X. M.; Huang, Y. F.; Ren, B.; Xu, X.; Tian, Z. Q. Surface Catalytic Coupling Reaction of P-Mercaptoaniline Linking to Silver Nanostructures Responsible for Abnormal SERS Enhancement: A DFT Study. *J. Phys. Chem. C* **2009**, *113* (42), 18212–18222.

(22) Fang, Y.; Li, Y.; Xu, H.; Sun, M. Ascertaining P, P'-dimercaptoazobenzene Produced from P-Aminothiophenol by Selective Catalytic Coupling Reaction on Silver Nanoparticles. *Langmuir* **2010**, *26* (11), 7737–7746.

(23) Xu, P.; Kang, L.; Mack, N. H.; Schanze, K. S.; Han, X.; Wang, H.-L. Mechanistic Understanding of Surface Plasmon Assisted Catalysis on a Single Particle: Cyclic Redox of 4-Aminothiophenol. *Sci. Rep.* **2013**, *3*, 2997.

(24) Liu, X.; Tang, L.; Niessner, R.; Ying, Y.; Haisch, C. Nitrite-Triggered Surface Plasmon-Assisted Catalytic Conversion of P-Aminothiophenol to P, p'-Dimercaptoazobenzene on Gold Nanoparticle: Surface-Enhanced Raman Scattering Investigation and Potential for Nitrite Detection. *Anal. Chem.* **2015**, *87*, 499–506.

(25) Long, D. A. *The Raman Effect: A Unified Treatment of the Theory of Raman Scattering by Molecules*; John Wiley & Sons, Inc.: West Sussex, 2002.

(26) Ferraro, J. R.; Nakamoto, K. *Introductory Raman Spectroscopy*; Academic Press, Inc.: San Diego, 1994.

(27) Bantz, K. C.; Meyer, A. F.; Wittenberg, N. J.; Im, H.; Kurtulus, O.; Lee, S. H.; Lindquist, N. C.; Oh, S.-H.; Haynes, C. L. Recent Progress in SERS Biosensing. **2011**, *13* (24), 11551–11567.

(28) Fleischmann, M.; Hendra, P. J.; McQuillan, A. J. Raman Spectra of Pyridine Adsorbed at a Silver Electrode. *Chem. Phys. Lett.* **1974**, *26* (2), 163–166.

(29) Jeanmaire, D. L.; Van Duyne, R. P. Surface Raman Spectroelectrochemistry. *Journal of Electroanalytical Chemistry and Interfacial Electrochemistry*. 1977, pp 1–20.

(30) Kneipp, K.; Kneipp, H.; Itzkan, I.; Dasari, R. R.; Feld, M. S. Surface-Enhanced Raman Scattering and Biophysics. *J. Physics-Condensed Matter* **2002**, *14* (18), R597–R624.

(31) Stiles, P. L.; Dieringer, J. A.; Shah, N. C.; Van Duyne, R. P. Surface-Enhanced Raman Spectroscopy. *Annu. Rev. Anal. Chem.* **2008**, *1* (1), 601–626.

(32) Wang, J. *Analytical Electrochemistry*, 2nd ed.; Wiley-VCH: New York, 2000.

(33)   Bard, A. J.; Faulkner, L. R. *Electrochemical Methods: Fundamentals and Applications*, 2nd ed.; John Wiley & Sons, Inc.: New York, 2001.

(34)   Hamann, C. H.; Hamnett, A.; Vielstich, W. *Electrochemistry*, 2nd ed.; Wiley-VCH: Weinheim, 2007.

(35)   Zhao, L.; Blackburn, J.; Brosseau, C. L. Quantitative Detection of Uric Acid by Electrochemical-Surface Enhanced Raman Spectroscopy Using a Multilayered Au/Ag Substrate. *Anal. Chem.* **2015**, *87* (1), 441–447.

(36)   Robinson, A. M.; Harroun, S. G.; Bergman, J.; Brosseau, C. L. Portable Electrochemical Surface-Enhanced Raman Spectroscopy System for Routine Spectroelectrochemical Analysis. *Anal. Chem.* **2012**, *84* (3), 1760–1764.

(37)   Fulmer, G. R.; Miller, A. J. M.; Sherden, N. H.; Gottlieb, H. E.; Nudelman, A.; Stoltz, B. M.; Bercaw, J. E.; Goldberg, K. I. NMR Chemical Shifts of Trace Impurities: Common Laboratory Solvents, Organics, and Gases in Deuterated Solvents Relevant to the Organometallic Chemist. *Organometallics* **2010**, *29* (9), 2176–2179.

(38)   Teke, M.; Sayıklı, Ç.; Canbaz, Ç.; Sezgintürk, M. K. A Novel Biosensing System Using Biological Receptor for Analysis of Vascular Endothelial Growth Factor. *Int. J. Pept. Res. Ther.* **2013**, *20* (2), 221–230.

(39)   Ma, D.; Zheng, J.; Tang, P.; Xu, W.; Qing, Z.; Yang, S.; Li, J.; Yang, R. Quantitative Monitoring of Hypoxia-Induced Intracellular Acidification in Lung Tumor Cells and Tissues Using Activatable Surface-Enhanced Raman Scattering Nanoprobes. *Anal. Chem.* **2016**, *88* (23), 11852–11859.

(40)   Pal, J.; Ganguly, M.; Dutta, S.; Mondal, C.; Negishi, Y.; Pal, T. Hierarchical Au–

CuO Nanocomposite from Redox Transformation Reaction for Surface Enhanced Raman Scattering and Clock Reaction. *CrystEngComm* **2014**, *16* (5), 883.

(41) Lang, X. F.; Yin, P. G.; Tan, E. Z.; You, T. T.; Guo, L. Theoretical Investigation on Surface-Enhanced Raman Evidence for Conformation Transition of Dimercaptoazobenzene Adsorbed on Gold Nanoclusters. *J. Raman Spectrosc.* **2013**, *44* (3), 425–432.

(42) Smaali, K.; Lenfant, S.; Karpe, S.; Oçafrain, M.; Blanchard, P.; Deresmes, D.; Godey, S.; Rochefort, A.; Roncali, J.; Vuillaume, D. High on-off Conductance Switching Ratio in Optically-Driven Self-Assembled Conjugated Molecular Systems. *ACS Nano* **2010**, *4* (4), 2411–2421.

(43) Alemani, M.; Peters, M. V.; Hecht, S.; Rieder, K. H.; Moresco, F.; Grill, L. Electric Field-Induced Isomerization of Azobenzene by STM. *J. Am. Chem. Soc.* **2006**, *128* (45), 14446–14447.

Appendix

Table A.1: Peak assignments for the calculated Raman data for cis and trans 3,3'-dimercaptoazobenzene.

Calculated Raman peaks/ cm^{-1} TRANS	Calculated Raman peaks/ cm^{-1} CIS	Peak Assignment
-	193	Ring def.
-	310	δ(C-S)
-	431	δ(C=C-H)
-	641	δ(N=N) + Ring def.
1017	1017	δ(S-H)
-	1160	ν(C-N)
1169	-	Ring def.
1203	-	Ring def.
1446	-	ν(C-S) + δ(C=C)
1528	-	δ(C-N=N) + mixed vibrations
-	1580	ν(N=N)

ν, stretching; δ, bending;

Table A.2: Peak assignments for the calculated Raman data for cis and trans 2,2'-dimercaptoazobenzene.

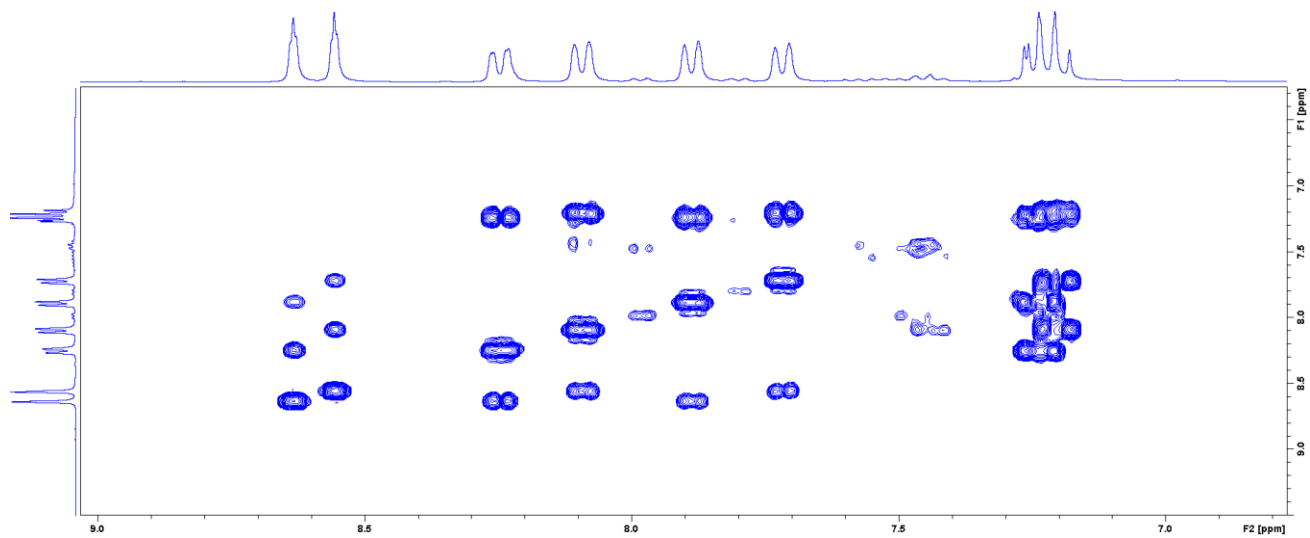| Calculated Raman peaks/ cm^{-1} TRANS	Calculated Raman peaks/ cm^{-1} CIS	Peak Assignment
-	239	-
-	286	δ(S-H)
-	342	Ring def.
-	487	Ring def.
-	629	Ring def. + δ(C-N=N)
914	-	δ(S-H)
1059	-	Ring def.
-	1059	ν(C=C)+ν(C-S)
-	1133	ν(C=C)+ν(C-S)
1135	-	Ring def.
1190	1182	ν(C-N) + ν(C-C)
1446	-	ν(N=N)
1523	1567	ν(N=N) + ν(C=C)

ν, stretching; δ, bending;

Figure A.2: COSY spectrum obtained from the synthesize product in CD$_2$Cl$_2$.